

Fig. 7. The frequency dependence of the complex permittivity, ε^* , at low temperature between -50 and $-10\,^{\circ}\text{C}$ for (a.1)–(a.2) CCTO_PC600, (b.1)–(b.2) CCTO_PC700 and (c.1)–(c.2) CCTO_PC800, respectively. (a.1)–(c.1) display the real part ε' ; (a.2)–(c.2) display the imaginary part ε'' .

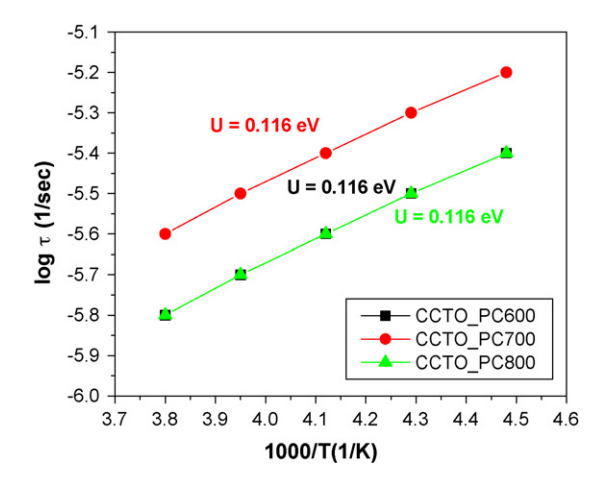


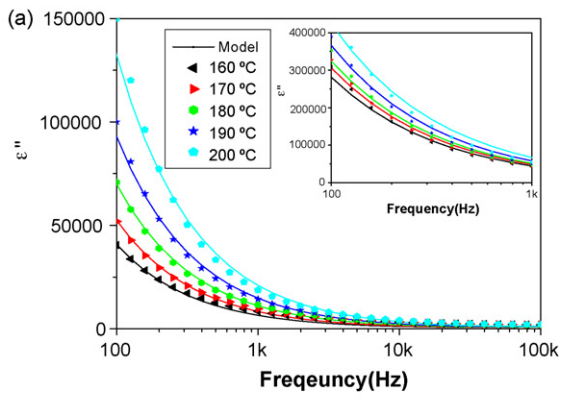
Fig. 8. Arrhenius plot of dielectric relaxation time τ for the three sintered samples.

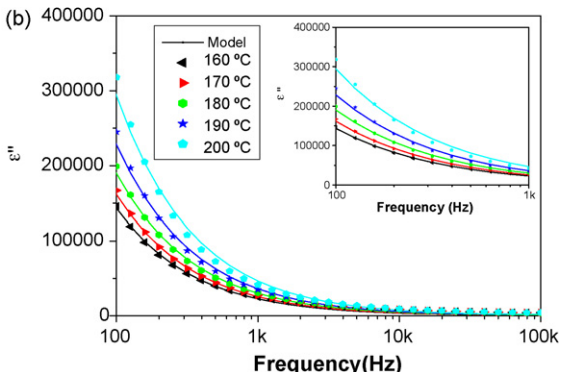
To interpret the dielectric in the CCTO ceramics, the Maxwell–Wagner relaxation was used to describe a series array of two sub-circuits, one in the grain and the other at the grain boundaries [13,43]. In each sub-circuit, the resistor and capacitor are in parallel. In this circuit, we can present the static-permittivity, ε_s' , and dielectric relaxation time, τ , in the following form

$$\varepsilon_{\rm s}' = \frac{R_{\rm g}^2 C_{\rm g} + R_{\rm gb}^2 C_{\rm gb}}{C_0 (R_{\rm g} + R_{\rm gb})^2} \tag{8}$$

$$\tau = \frac{R_g R_{gb} (C_g + C_{gb})}{R_g + R_{gb}} \tag{9}$$

where $C_{\rm g}$ and $C_{\rm gb}$ are the capacitance of grain and grain boundaries, respectively; $R_{\rm g}$ and $R_{\rm gb}$ are the resistor of grain and grain boundaries, respectively; C_0 is the empty cell constant and τ is the time constant.





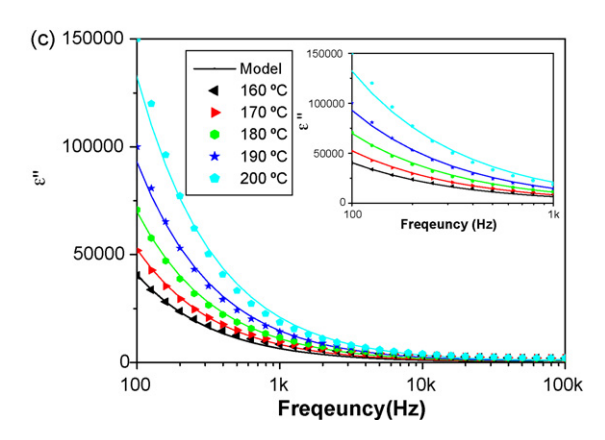


Fig. 9. The frequency dependence of the dielectric loss ε'' at high temperature ranging between 160 and 200 °C for (a) CCTO_PC600, (b) CCTO_PC700 and (c) CCTO_PC800, respectively. The solid lines are the fits according to Eq. (6).

It has been reported in the literature that for CCTO, $R_{\rm gb} \gg R_{\rm g}$ and $C_{\rm gb} \approx 10~C_{\rm g}$ [13,43]. We can estimate the static-permittivity $\varepsilon_{\rm s}'$ from Eq. (8),

$$\varepsilon_{\rm s}' pprox rac{C_{
m gb}}{C_0}$$
 (10)

Thus, ε_s' is determined by the ratio between grain boundary capacitance, $C_{\rm gb}$, and empty cell capacitance, C_0 . Hence ε_s' is constant when $C_{\rm gb}$ is temperature and frequency independent. The implication is in good agreement with our experimental results. We observed that dielectric constant is not dependent on the frequency and only weakly dependent on the temperature.

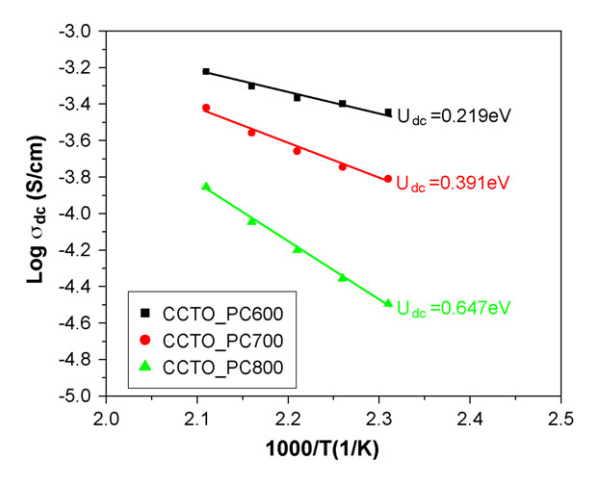


Fig. 10. Arrhenius plot of dc conductivity σ_{dc} for the three sintered samples.

If we assumed that the grain boundary form a two-layer capacitor with a thickness of $(d_{\rm g}+d_{\rm gb})$, where $d_{\rm g}$ and $d_{\rm gb}$ are the thickness of the grain and the grain boundary layer, respectively, from Eq. (10), one obtains $\varepsilon_{\rm s}'\approx \varepsilon_{\rm gb}(d_{\rm g}+d_{\rm gb})/d_{\rm gb}$; here $\varepsilon_{\rm gb}$ is the dielectric constant of the grain boundary layer. Therefore, even a small dielectric constant $\varepsilon_{\rm gb}$ can lead to a giant dielectric constant $\varepsilon_{\rm s}'$ if the ratio $(d_{\rm g}+d_{\rm gb})/d_{\rm gb}$ is large. If the grain is about 10 μ m, the grain boundary layer is about 0.01 μ m and $\varepsilon_{\rm gb}=10$, then $\varepsilon_{\rm s}'\approx 10$, 000. Therefore, the Maxwell–Wagner relaxation can be used to explain the giant dielectric constant of our CCTO samples.

Using the conditions, $R_{\rm gb} \gg R_{\rm g}$ and $C_{\rm gb} \approx 10~C_{\rm g}$ [13,43]. We can approximately obtain the time constant, τ , from Eq. (9),

$$\tau \approx R_{\rm g}C_{\rm gb} = (R_{\rm g}C_{\rm g})\frac{C_{\rm gb}}{C_{\rm o}} = \tau_{\rm g}\frac{C_{\rm gb}}{C_{\rm o}}$$
(11)

where $\tau_g = R_g C_g$ is the response time of the grain. It has been reported that C_g and C_{gb} are independent of temperature [11,43], thus, we can deduce τ_g that follows the Arrhenius law, Eq. (5). Let $\tau_g = \tau_g^0 \exp(U_g/k_BT)$ (τ_g^0 is pre-exponential factor and U_g is the activation energy of the grain conduction process), then we modify Eq. (11) to

$$\tau \approx R_{\rm g} C_{\rm gb} = \frac{C_{\rm gb}}{C_{\rm g}} \left(\tau_{\rm g}^0 \exp\left(\frac{U_{\rm g}}{k_{\rm B} T}\right) \right) \tag{12}$$

From Eq. (12), τ and τ_0 have the same temperature dependence and the electrical response of the grains has the same activation energy as that of the observed dielectric relaxation. Thus, we can conclude that the activation energy for the response of the grains in CCTO_PC600, CCTO_PC700 and CCTO_PC800 are 0.116 eV, which are close to the values of 0.109 eV for a chemical solution synthesized CCTO and 0.112 eV for the recently reported by our group [14]. However, the value of 0.116 eV is lager than 0.08 eV, which was reported for samples made by solid-state reaction [11]. The activation energy of grain in CCTO_PC600, CCTO_PC700 and CCTO_PC800 are lager than activation energy of grain in sample made by solid-state reaction, which may imply that there are fewer oxygen vacancies in the grains of CCTO_PC600,

CCTO_PC700 and CCTO_PC800. This is reasonable because CCTO_PC600, CCTO_PC700 and CCTO_PC800 were sintered from powders. These powders were calcined at low temperature (600, 700 and 800 °C) compared to the temperature needed for the solid-state processing, which calcined at 1000 °C [11]. Similar suggestion was explained by Liu et al. [13].

4. Conclusions

Nanocrystalline CaCu $_3$ Ti $_4$ O $_{12}$ powders with particle sizes of 30–100 nm have been synthesized by the polymerized complex route. The powders were used to prepared bulk CCTO ceramics, which exhibit giant dielectric response and have the dielectric constant as high as 10,000–20,000 at 1 kHz. The dielectric constant is weakly temperature dependent over the temperature range of $-50\,^{\circ}$ C to $200\,^{\circ}$ C. The high dielectric-constant responses of these CCTO ceramics are not attributed to the ferroelectric behavior, but rather to the Maxwell–Wagner polarization mechanism.

Acknowledgements

The authors would like to thank the Department of Chemistry for providing TG-DTA and FT-IR facilities, the Faculty of Science Electron Microscopy Unit for providing SEM facilities. C. Masingboon would like to thank the University Staff Development Program, Kasetsart University Chalermphrakiat Sakon Nakhon Province Campus, Thailand for financial support. Assistance from Mr. Phillip Anderson, the University of Arizona, on TEM analysis is gratefully acknowledged. This work is supported by the National Science and Technology Development Agency (NSTDA), Thailand (under contact no. F-31-401-12-02).

References

- A.P. Ramirez, M.A. Subramanian, M. Gardel, G. Blumberg, D. Li, T. Vogt, S.M. Shapiro, Solid State Commun. 115 (2000) 217.
- [2] M.A. Subramanian, L. Dong, N. Duan, B.A. Reisner, A.W. Sleight, J. Solid State Chem. 151 (2000) 323.
- [3] C.C. Homes, T. Vogt, S.M. Shapiro, S. Wakimoto, A.P. Ramirez, Science 293 (2001) 73.
- [4] A.F.L. Almeida, R.S. de Oliveira, J.C. Góes, J.M. Sasaki, A.G. Souza Filho, J. Mendes Filho, A.S.B. Sombra, Mater. Sci. Eng. B 96 (2002) 275.
- [5] M.A. Subramanian, A.W. Sleight, Solid State Sci. 4 (2002) 347.
- [6] Z. Yu, C. Ang, J. Appl. Phys. 91 (2002) 794.
- [7] L. Fang, M.R. Shen, Thin Solid Films 440 (2003) 60.
- [8] P. Jha, P. Arora, A.K. Ganguli, Mater. Lett. 57 (2003) 2443.

- [9] J. Li, A.W. Sleight, M.A. Subramanian, Solid State Commun. 135 (2005) 260.
- [10] S. Jin, H. Xia, Y. Zhang, J. Guo, J. Xu, Mater. Lett. 61 (2007) 1404.
- [11] D.C. Sinclair, T.B. Adams, F.D. Morrison, A.R. West, Appl. Phys. Lett. 80 (2002) 2153.
- [12] B.A. Bender, M.J. Pan, Mater. Sci. Eng. B 117 (2005) 339.
- [13] J. Liu, Y. Sui, C. Duan, W.N. Mei, R.W. Smith, J.R. Hardy, Chem. Mater. 18 (2006) 3878.
- [14] P. Thongbai, C. Masingboon, S. Maensiri, T. Yamwong, S. Wongsaenmai, R. Yimnirun, J. Phys. Condens. Matter 19 (2007) 236208.
- [15] S. Chung, I. Kim, S. Kang, Nat. Mater. 3 (2006) 774.
- [16] T.T. Fang, H.K. Shiau, J. Am. Ceram. Soc. 87 (2004) 2072.
- [17] S.F. Shao, J.L. Zhang, P. Zheng, W.L. Zhong, C.L. Wang, J. Appl. Phys. 99 (2006) 084106.
- [18] P. Lunkenheimer, V. Bobnar, A. V. Pronin, A.I. Ritus, A.A. Volkov, A. Loidl, Phys. Rev. B 66 (2002) 052105.
- [19] P. Lunkenheimer, R. Fichtl, S.G. Ebbinghaus, A. Loidl, Phys. Rev. B 70 (2004) 172102.
- [20] M.H. Cohen, J.B. Neaton, L.X. He, D. Vanderbilt, J. Appl. Phys. 94 (2003) 3299.
- [21] L. Zhang, Z.J. Tang, Phys. Rev. B 70 (2004) 174306.
- [22] A.R. West, T.B. Adams, F.D. Morrison, D.C. Sinclair, J. Eur. Ceram. Soc. 24 (2004) 1439.
- [23] G. Chiodeli, V. Massarotti, D. Capsoni, M. Bini, C.B. Azzoni, M.C. Mozzati, P. Lupotto, Solid State Commun. 132 (2004) 241.
- [24] D. Capsoni, M. Bini, V. Massarotti, G. Chiodelli, M.C. Mozzatic, C.B. Azzoni, J. Solid State Chem. 177 (2004) 4494.
- [25] S.V. Kalinin, J. Shin, G.M. Veith, A.P. Baddorf, M.V. Lobanov, H. Runge, M. Greenblatt, Appl. Phys. Lett. 86 (2005) 102902.
- [26] T.T. Fang, L.T. Mei, H.F. Ho, Acta Mater. 54 (2006) 2867.
- [27] M.P. Pechini, US Patent 3,330,697, (1967).
- [28] P.A. Lessing, Am. Ceram. Soc. Bull. 168 (1989) 1002.
- [29] M. Kakihana, J. Sol Gel Sci. Technol. 6 (1996) 7.
- [30] M. Kakihana, M. Arima, Y. Nakamura, M. Yashima, M. Yoshimura, Chem. Mater. 11 (1999) 438.
- [31] R.A. Rocha, E.N.S. Muccillo, Chem. Mater. 115 (2003) 4268.
- [32] M. Vijayakumar, Y. Inaguma, W. Mashiko, M.P. Crosnier-Lopez, C. Bohnke, Chem. Mater. 16 (2004) 2719.
- [33] T. Seretawa, V. Amornkitbamrung, T. Burinprakhon, S. Maensiri, Inter. J. Nanosci. 4 (2005) 237.
- [34] S. Maensiri, P. Thongbai, T. Yamwong, Acta Mater. 55 (2007) 2851.
- [35] K. Wongsaprom, E. Swatsitang, S. Srijaranai, S. Maensiri, S. Seraphin, Appl. Phys. Lett. 90 (2007) 162506.
- [36] S. Guillemet-Fritsch, T. Lebey, M. Boulos, B. Durand, J. Eur. Ceram. Soc. 26 (2006) 1245.
- [37] B.D. Cullity, S.R. Stock, Elements of X-ray Diffraction, Prentice Hall, Englewood Cliffs, 2001.
- [38] P. Leret, J.F. Fernandez, J. de Frutos, D. Fernández-Hevia, J. Eur. Ceram. Soc. 27 (2007) 3901.
- [39] C.K. Yeoh, M.F. Ahmad, Z.A. Ahmad, J. Alloys Compd. 443 (2007) 155.
- [40] M.A. Ramirez, P.R. Bueno, J.A. Varela, E. Longo, Appl. Phys. Lett. 89 (2006) 212102.
- [41] K.C. Kao, Dielectric Phenomena in Solids, Elsevier Academic Press, London, 2004.
- [42] J. Wu, C.W. Nan, Y. Lin, Y. Deng, Phys. Rev. Lett. 89 (2002) 217601.
- [43] J. Liu, C.G. Duan, W.G. Yin, W.N. Mei, R.W. Smith, J.R. Hardy, Phys. Rev. B 70 (2004) 144106.

Materials Science & Processing

DOI: 10.1007/s00339-007-4363-4

C. MASINGBOON¹
S. MAENSIRI^{1, \boxtimes}
T. YAMWONG²
P.L. ANDERSON³
S. SERAPHIN³

Nanocrystalline CaCu₃Ti₄O₁₂ powders prepared by egg white solution route: synthesis, characterization and its giant dielectric properties

- ¹ Small & Strong Materials Group (SSMG), Department of Physics, and Integrated Nanotechnology Research Center (INRC), Faculty of Science, Khon Kaen University, Khon Kaen 40002, Thailand
- National Metals and Materials Technology Center (MTEC), Thailand Science Park, Pathumthani 12120, Thailand
- ³ Department of Materials Science and Engineering, The University of Arizona, Tucson, AZ 85721, USA

Received: 20 June 2007/Accepted: 19 November 2007 Published online: 19 December 2007 • © Springer-Verlag 2007

ABSTRACT Nanocrystalline CaCu₃Ti₄O₁₂ powders with particle sizes of 50-90 nm were synthesized by a simple method using Ca(NO₃)₂·4H₂O, Cu(NO₃)₂·4H₂O, titanium(diisoproproxide) bis(2,4-pentanedionate) and freshly extracted egg white (ovalbumin) in aqueous medium. The synthesized precursor was characterized by TG-DTA to determine the thermal decomposition and crystallization temperature which was found to be at above 400 °C. The precursor was calcined at 700 and 800 °C in air for 8 h to obtain nanocrystalline powders of CaCu₃Ti₄O₁₂. The calcined CaCu₃Ti₄O₁₂ powders were characterized by XRD, FTIR, SEM and TEM. Sintering of the powders was conducted in air at 1100 °C for 16 h. The XRD results indicated that all sintered samples have a typical perovskite CaCu₃Ti₄O₁₂ structure and a small amount of CuO, although the sintered sample of the 700 °C calcined powders contained some amount of CaTiO₃. SEM micrographs showed the average grain sizes of 12.0 ± 7.8 and 15.5 ± 8.9 µm for the sintered CaCu₃Ti₄O₁₂ ceramics prepared using the CaCu₃Ti₄O₁₂ powders calcined at 700 and 800 °C, respectively. The sintered samples exhibit a giant dielectric constant, ε' of $\sim 1.5-5 \times 10^4$. The dielectric behavior of both samples exhibits Debye-like relaxation, and can be explained based on a Maxwell-Wagner model.

PACS 77.22.Gm; 81.05.Je; 81.07.Wx; 81.20.Ev

1 Introduction

Materials with high dielectric constant, good thermal stability and Ba/Pb-free are widely used in technological applications such as capacitors and memory devices. Recently, there has been a great interest in synthesis and characterization of a perovskite-type compound, CaCu₃Ti₄O₁₂, (abbreviated as CCTO) [1–15]. This non-ferroelectric material exhibits giant dielectric constant of $\varepsilon' \sim 10^4$ (for polycrystalline ceramics) [1, 2] and $\varepsilon' \sim 10^5$ (for single crystals) [3] in the kilohertz region over the temperature range from -173 to

327 °C. This material does not undergo any structural change over the same temperature range [1, 2] although its dielectric constant abruptly decreases to less than 100 below -173 °C and shows a Debye-like relaxation [13]. The characteristic relaxation frequency follows approximately the Arrhenius law. In addition to its interesting dielectric property, CCTO has remarkably strong linear current–voltage characteristics without the addition of dopants [16]. These excellent properties render this material particularly attractive for a wide range of applications.

So far, several models of the dielectric behavior of CCTO material have been proposed to be due to either intrinsic or extrinsic effect. Since the giant dielectric response of this material was found to be very sensitive to the microstructure (such as grain size) and processing conditions (such as sintering temperature and time, cooling rate, and partial pressure) [11–14, 17, 18], more investigations tend to believe that the high dielectric constant originates from the extrinsic effect, such as internal barrier layer capacitor (IBLC) [11, 17], contact-electrode effect [19, 20], and special inhomogenity of local dielectric response [21]. Although still unclear, the IBLC explanation of extrinsic mechanism is widely accepted [22–27].

CCTO powder was generally prepared by a standard solid-state reaction method [1–3]. This method requires tedious work and a high temperature in the powder preparation process. Moreover, it suffers from the disadvantages of inhomogeneity. In contrast, synthesis from a solution affords the reaction with a homogeneous mixing of the metal ions at the atomic scale, shorter reaction time, and at lower temperature in the powder preparation process [28].

However, it has been only a few reports on the solution methods to synthesize CCTO powders [8, 10, 13]. Therefore, alternative simple solution routes by utilization of cheap, nontoxic and environmentally benign precursors for preparation of CCTO powders are still a challenge. Egg white proteins are well known for their gelling, foaming and emulsifying characteristics, in addition to their high nutrition quality [29–31]. Due to its solubility in water and its ability to associate with metal ions in solution, egg white has been used as a binder cum gel forming material in shape form-

ing of bulk and porous ceramics [32–34]. Egg white has been used as a matrix for entrapment of aluminum ions generating gel precursor which resulted in α -alumina particles with crystalline sizes of 15–80 nm after heat treatment as low as 330 °C [35]. Most recently, our group has reported the use of egg white solution for the preparations of plate-like clusters of CeO₂ nanocrystalline particles 6–30 nm in diameter [36] and nanoparticles of NiFe₂O₄ with particle sizes of 60–600 nm [37]. This method is simple, cost effective and environmental friendly, which is a promising synthesis route for preparation of fine ceramic particles.

In this study, we report the synthesis and giant dielectric properties of CCTO prepared by the simple egg white solution route using Ca(NO₃)₂·4H₂O, Cu(NO₃)₂·4H₂O, titanium(diisoproproxide) bis(2,4-pentanedionate) and freshly extracted egg white (ovalbumin) in aqueous medium. The synthesized fine CCTO powders were characterized by thermogravimetric and differential thermal analysis (TG-DTA), X-ray diffraction (XRD), Fourier-transform infared (FT-IR) spectroscopy, scanning electron microscopy (SEM) and transmission electron microscopy (TEM). The effects of particle size of the synthesized powders on microstructure and giant dielectric behavior of the sintered CCTO were also investigated.

2 Experimental procedure

The nanocrystalline CCTO powders were prepared by a simple egg white solution route. The procedures used to synthesize the CCTO powders were similar to those for the NiFe₂O₄ nanoparticles reported previously [37]. In a typical procedure, 60 ml of egg white was first mixed with 40 ml de-ionized water (3:2 ratio) under vigorous stir at room temperature (27 °C) until homogeneous solution was obtained. Subsequently, Ca(NO₃)₂·4H₂O (99.9% purity, Kento, Japan), Cu(NO₃)₂·4H₂O (99.5% purity, Carlo Erba Reacgenti, Italy), and 75 wt. % titanium(diisopropoxide) bis(2,4-pentanedionate) in 2-propanol (99%, Acros organics, USA) in a mole ratio corresponding to the nominal composition of CaCu₃Ti₄O₁₂. These chemicals were added to the egg white solution under vigorous stir at room temperature for 2 h to obtain a well-dissolved solution. At this step, the extracted egg white was acted as a matrix for entrapment of Ca, Cu, and Ti ions generating gel precursor [35-37]. Throughout the whole process described above, no pH adjustment was made. Then, the mixed solution was evaporated by heating on a hot plate at 100 °C under vigorous stir for several hours until dried precursor was obtained. The dried precursor was crushed into powder using mortar and pestle.

In order to determine the temperature of possible decomposition and crystallization of the nanoparticles, the dried precursor was subjected to thermogravimetric-differential thermal analysis (TG-DTA) (Pyris Diamond TG-DTA, Perkin–Elmer Instrument, USA). The crystallization seemed to occur at temperature above 400 °C (Fig. 1). The dried precursor then was calcined in box-furnace at 700 and 800 °C for 8 h in air. The calcined powder precursors were reground and passed through 106 μ m sieve (Test sieve, Endecotts Limited, England) to break up large agglomerates.

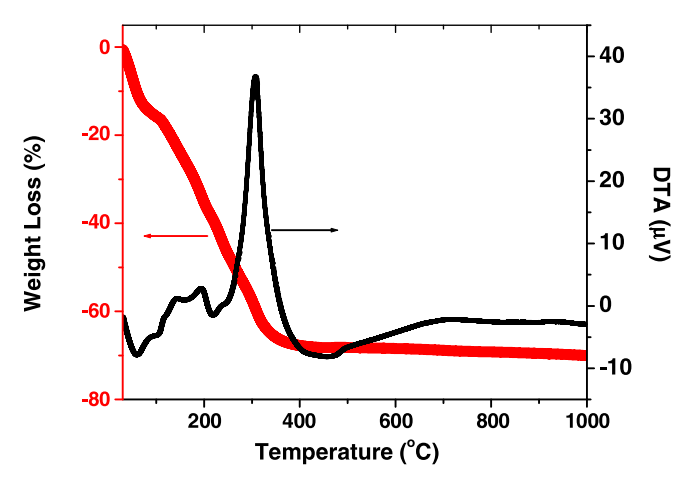


FIGURE 1 The TG/DTA curves of the thermal decomposition of CaCu $_3$ Ti $_4$ O $_{12}$ precursor at a heating rate of 15 $^\circ$ C/min in static air

The prepared CCTO powers were characterized by X-ray diffraction (PW3040 Philips X-ray diffractometer with Cu K_{α} radiation ($\lambda=0.15406$ nm), The Netherlands), Fourier transform infrared spectrometer (Spectrum One FT-IR Spectrometer, Perkin–Elmer Instruments, USA), scanning electron microscopy (LEO SEM VP1450, UK) and transmission electron microscopy (TEM, Hitachi H8100 200 kV).

The prepared powders were pressed uniaxially in a 16 mm die with an applied pressure of 100 MPa. The compacts were pressureless-sintered at $1100\,^{\circ}\text{C}$ for 16 h in air in a box furnace with heating and cooling rates of $5\,^{\circ}\text{C/min}$. The sintered disc samples of ~ 14 mm in diameter with a thickness of ~ 2 mm were obtained. The average grain size of each sintered CCTO ceramic was measured using a standard line intercept technique from SEM micrographs of sintered CCTO surfaces and counting at least 200 intercepts for each micrograph. Throughout this article, we assigned symbols of CCTO_EW700 and CCTO_EW800 for the sintered CCTO samples fabricated using the CCTO powders calcined at 700 and 800 °C, respectively.

The capacitance, C, and loss tangent, $\tan \delta$, were carried out as a function of frequency (100 Hz–10 MHz) and temperature (–50 to +190 °C), using a Hewlett Packard 4194A Impedance Gain Phase Analyzer at an oscillation voltage of 1 V. Each measured temperature was kept constant with an accuracy of ± 1 °C. Silver paint was coated on both surface of the samples and dried over night. The complex permittivity, ε^* , was calculated as follows:

$$\varepsilon^* = \varepsilon' - i\varepsilon'' \,, \tag{1}$$

where

$$\varepsilon' = \frac{Cd}{\varepsilon_0 A} \,, \tag{2}$$

$$\varepsilon'' = \varepsilon' \tan \delta \,, \tag{3}$$

where ε_0 is the permittivity in free space, A is the sample area and d is the sample thickness. The values of ac conductivity, σ_{ac} , were derived from [38]:

$$\sigma_{\rm ac} = \omega \varepsilon_0 \varepsilon'' \,. \tag{4}$$

3 Results and discussion

The simultaneous TG-DTA curves of the gel precursor in flowing air are shown in Fig. 1. The TG curve in Fig. 1 shows a minor weight loss step between ~ 30 °C and 300 °C. A slight weight loss was observed between 300 and 400 °C, and almost no weight loss was observed at above 500 °C. The first weight loss (30–300 °C) is related to the losses of moisture, trapped solvent (water and carbon dioxide), alkoxide, and nitrates. A slightly weight loss was observed between 300 and 400 °C, relating to the losses of organic species associated in the precursor (the remaining organic mass in ovalbumin), or the residual carbon. Almost no weight loss could be observed at above 400 °C, suggesting the formation of crystalline CCTO as a decomposed product. This is confirmed by the XRD results as shown in Fig. 2. On the DTA curve (Fig. 1) three endothermic peaks were observed at \sim 57, 103, and 219 °C, respectively. The one exothermic was observed at 304 °C. The three endothermic peak confirms the combustion of water, whereas the one exothermic peak confirms that the thermal events was associated with the burnout of organic species involved in the precursor powders of the residual carbon or due to direct crystallization of CCTO from the amorphous component. No further weight loss and no thermal effect were observed above 400 °C, indicating that no decomposition occurs above this temperature. Note that this precursor was calcined in air at 700 and 800 °C for 8 h.

Figure 2 shows XRD patterns of (a) dried precursor and CCTO powders after calcination in air at (b) 700 °C and (c) 800 °C for 8 h. The main peaks of all calcined CCTO powders are comparable to those of the standard powder XRD pattern of CCTO in the JCPDS card No. 75-2188. In addition, the following phases of CaTiO₃ (JCPDS card No. 82-0228), CuO (JCPDS card No. 80-0076) and Anateses-TiO₂ (JCPDS card No. 78-2486) are also observed. It is suggested by Guilleemet-Fritsch et al. [39] that the pure CCTO phase is obtained only when the ratio of calcium, copper and titanium are close to the stoichiometric ones. The CaTiO₃ phase appears if an ex-

Intensity(a.u.)

A

(013)

(125)

(125)

(125)

(125)

(125)

(125)

(125)

(126)

(127)

(127)

(128)

(129)

(129)

(129)

(129)

(129)

(129)

(129)

(129)

(129)

(129)

(129)

(129)

(129)

(129)

(129)

(129)

(129)

(129)

(129)

(129)

(129)

(129)

(129)

(129)

(129)

(129)

(129)

(129)

(129)

(129)

(129)

(129)

(129)

(129)

(129)

(129)

(129)

(129)

(129)

(129)

(129)

(129)

(129)

(129)

(129)

(129)

(129)

(129)

(129)

(129)

(129)

(129)

(129)

(129)

(129)

(129)

(129)

(129)

(129)

(129)

(129)

(129)

(129)

(129)

(129)

(129)

(129)

(129)

(129)

(129)

(129)

(129)

(129)

(129)

(129)

(129)

(129)

(129)

(129)

(129)

(129)

(129)

(129)

(129)

(129)

(129)

(129)

(129)

(129)

(129)

(129)

(129)

(129)

(129)

(129)

(129)

(129)

(129)

(129)

(129)

(129)

(129)

(129)

(129)

(129)

(129)

(129)

(129)

(129)

(129)

(129)

(129)

(129)

(129)

(129)

(129)

(129)

(129)

(129)

(129)

(129)

(129)

(129)

(129)

(129)

(129)

(129)

(129)

(129)

(129)

(129)

(129)

(129)

(129)

(129)

(129)

(129)

(129)

(129)

(129)

(129)

(129)

(129)

(129)

(129)

(129)

(129)

(129)

(129)

(129)

(129)

(129)

(129)

(129)

(129)

(129)

(129)

(129)

(129)

(129)

(129)

(129)

(129)

(129)

(129)

(129)

(129)

(129)

(129)

(129)

(129)

(129)

(129)

(129)

(129)

(129)

(129)

(129)

(129)

(129)

(129)

(129)

(129)

(129)

(129)

(129)

(129)

(129)

(129)

(129)

(129)

(129)

(129)

(129)

(129)

(129)

(129)

(129)

(129)

(129)

(129)

(129)

(129)

(129)

(129)

(129)

(129)

(129)

(129)

(129)

(129)

(129)

(129)

(129)

(129)

(129)

(129)

(129)

(129)

(129)

(129)

(129)

(129)

(129)

(129)

(129)

(129)

(129)

(129)

(129)

(129)

(129)

(129)

(129)

(129)

(129)

(129)

(129)

(129)

(129)

(129)

(129)

(129)

(129)

(129)

(129)

(129)

(129)

(129)

(129)

(129)

(129)

(129)

(129)

(129)

(129)

(129)

(129)

(129)

(129)

(129)

(129)

(129)

(129)

(129)

(129)

(129)

(129)

(129)

(129)

(129)

(129)

(129)

(129)

(129)

(129)

(129)

(12

FIGURE 2 XRD patterns of (**a**) dried precursor and $CaCu_3Ti_4O_{12}$ nanopowders calcined in air for 8 h at (**b**) 700 °C, and (**c**) 800 °C. (* – $CaTiO_3$, + – CuO, A – Anatase- TiO_2)

cess of titanium is present, and at the same time when the copper content slightly decreases. It is also suggested that the excess of titanium leads to the precipitation of CaTiO₃, even if there is no excess of calcium [39]. Since both calcium and titanium form a second phase, copper is then in excess, with respect with the stoichiometry of CCTO. Hence, the precipitation of the copper oxide (CuO) is observed, beside the CCTO and CaTiO₃ phase. From the line broadening of the main peaks, the crystallite size (*D*) was estimated using the Scherrer formula [40]:

$$D = K\lambda/(\beta\cos\theta), \tag{5}$$

where λ is the wavelength of the X-ray radiation, K is a constant taken as 0.89, θ is the diffraction angle. β is the full width at haft maximum (FWHM) and is given by $\beta = (\beta_o^2 - \beta_i^2)^{1/2}$, where β_o and β_i are the widths from the observed X-ray peak and the width due to instrumental effects, respectively. The particle sizes are found to be 66.7 ± 27.5 and 86.2 ± 35.2 nm for the powders calcined at 700 and $800\,^{\circ}$ C, respectively. The values of lattice parameter a calculated from the XRD spectra were obtained to be 7.374 ± 0.002 and 7.390 ± 0.0005 Å for the CCTO powders calcined at 700 and $800\,^{\circ}$ C, respectively. The particle sizes and lattice parameters are also summarized in Table 1.

Figure 3 shows FT-IR spectra of the dried precursor and CCTO powders after calcination in air at 700 °C and 800 °C for 8 h. The calcined CCTO powders show the main

Material	Particle size from XRD (nm)	Particle size from TEM (nm)	Lattice parameter <i>a</i> (Å)
ASTM (75-2188)	-	$-$ 56.7 \pm 7.9 84.9 \pm 15.3	7.391 ± 0.001
700 °C powders	66.7 ± 27.5		7.374 ± 0.002
800 °C powders	86.2 ± 35.2		7.390 ± 0.0005

TABLE 1 Summary of particle size analysis obtained from XRD and TEM; and lattice parameter (from XRD) of CCTO powders compared to the ASTM value

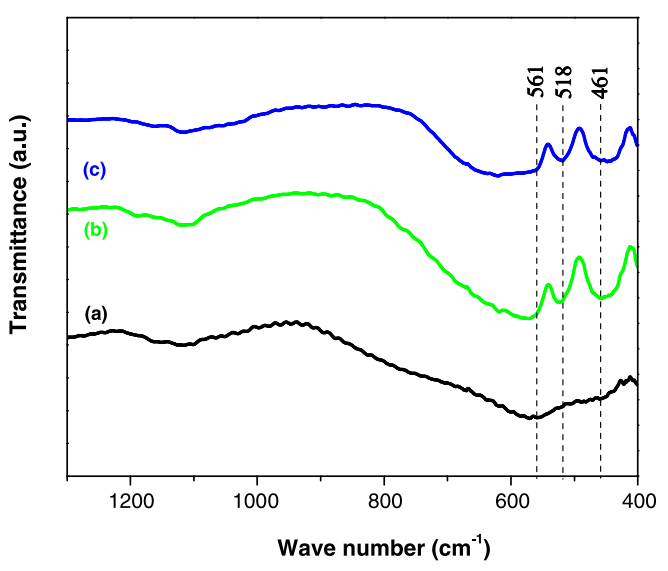


FIGURE 3 FT-IR patterns of (a) dried precursor and $CaCu_3Ti_4O_{12}$ nanopowders calcined in air for 8 h at (b) $700\,^{\circ}C$, and (c) $800\,^{\circ}C$

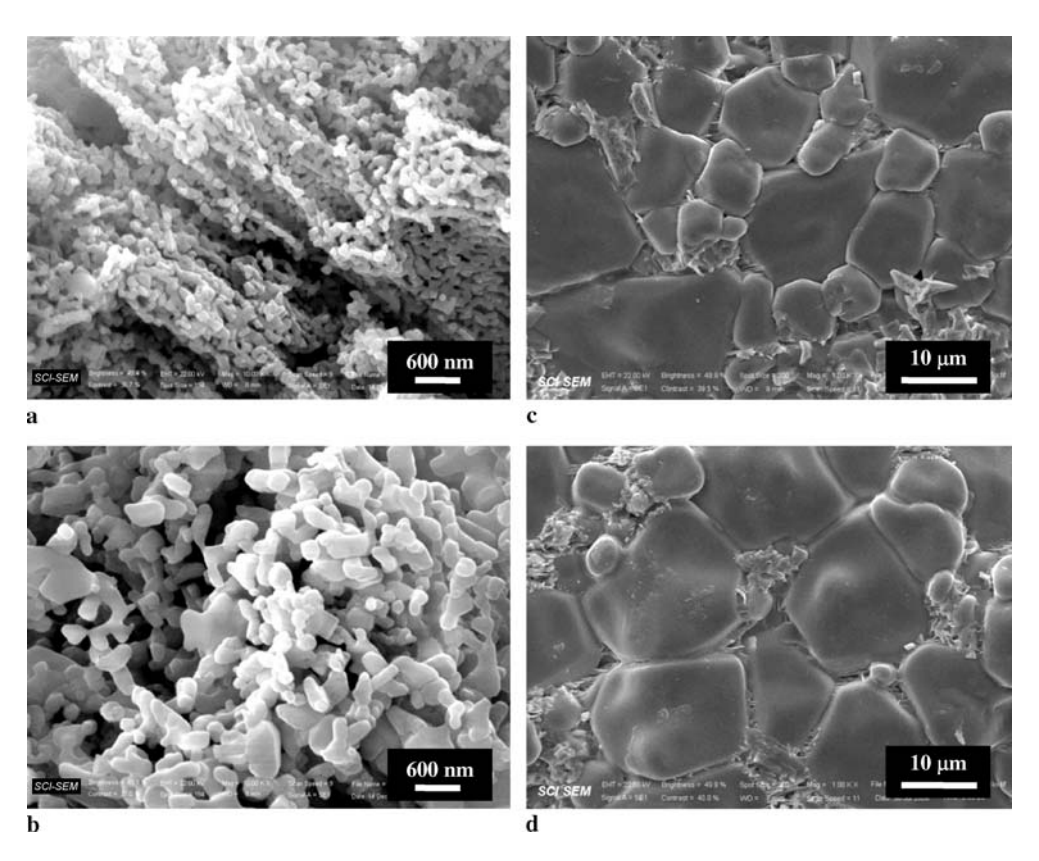


FIGURE 4 SEM micrographs of the CCTO powders and sintered CCTO materials. (a,b) are the powders calcined for 8 h in air at 700 °C and 800 °C, respectively. (c, d) are the microstructure of the sintering CCTO_EW700, and CCTO_EW800, respectively

absorption bands at 561, 516, and $437 \,\mathrm{cm}^{-1}$. These bands are assigned to the absorption regions for Ti ion, which are associated to $\nu_{\mathrm{Ti}-\mathrm{O}}$ of $653-550 \,\mathrm{cm}^{-1}$ and $(\mathrm{Ti}-\mathrm{O}-\mathrm{Ti})$ of $495-436 \,\mathrm{cm}^{-1}$ [4,41].

Morphology of the calcined CCTO powders and microstructure of the sintered CCTO ceramic samples revealed by SEM are shown in Fig. 4. Figure 4a and b show CCTO particles with sizes of about 60 nm, and 100 nm for the 700 °C and 800 °C calcined samples, respectively. These values were larger than those obtained from X-ray line broadening calculation. Some agglomerates were observed in all of the calcined powders. The particle size of the powder increased with increasing calcination temperature. After sintering at $1100\,^{\circ}\text{C}$ for 16 h, the bulk CCTO ceramics with different microstructure were obtained. The CCTO_EW700 (Fig. 4c) and CCTO_EW800 (Fig. 4d) showed mean grain sizes of $12.0\pm7.8\,\mu\text{m}$ and $15.5\pm8.9\,\mu\text{m}$, respectively.

Figure 5 shows TEM images and the corresponding selected area electron diffraction (SAED) patterns of the calcined CCTO powders. It is clearly seen from the TEM brightfield images that both powder samples consist of nanocrystalline CCTO particles, whose size increases with increasing calcination temperature. The 700 °C calcined sample contains nanoparticles of 56.7 ± 7.9 nm in size whereas the 800 °C calcined sample contains nanoparticles of 84.9 ± 15.3 nm. The observed particle sizes are in good agreement with results determined from X-ray line broadening (see summary in Table 1). Electron diffraction of particles with higher calcination temperature contains more intense spots as shown in the 800 °C calcined powders, indicating the larger particle size of highly crystalline compared to the 700 °C calcined samples. The interplanar spacings (d_{hkl}) measured from the

selected-area electron diffraction patterns are in good agreement with the values obtained from the standard data JCPDS: 75-2188 (for CCTO) and 89-0056 (for CaTiO₃) as summarized in Table 2.

Figure 6 shows XRD patterns of the CCTO ceramics sintered in air at 1100 °C for 16 h, confirming a main phase of CCTO and a small amount of CuO in both the CCTO EW700 and CCTO EW800 although a small amount of CaTiO₃ was present in the CCTO EW700 sample. The presence of additional CaTiO₃ in the sintered CCTO_EW700 is possibly due to the presence of excess titanium on the powders, calcined at 700 °C. Guilleemet-Fritsch et al. [39] suggested that the titanium content mostly controls the phase composition (single or second phase material) of the CCTO materials. Therefore, we think that the excess of titanium leads to the precipitation of CaTiO₃ in our CCTO_EW700 sample. In the case of CCTO_EW800, however, the CaTiO₃ phase is not observed. This implies that 800 °C – calcined powders have no excess of titanium. For the presence of the CuO phase in both the samples of CCTO_EW700 and CCTO_EW800, it is possible that the Cu rich phase derives from the diffusion of Cu to the defects present, after which gross excess causes the crystallization of the separate CuO phase [42]. The CuO phase within the ceramics implies that excess copper is in the form of a copper rich phase at the grain boundaries [43]. The values of lattice parameter a calculated from the XRD spectra were 7.388 ± 0.001 and 7.393 ± 0.001 Å for the CCTO_EW700 and CCTO_EW800, respectively (see summary in Table 3).

Figure 7a and b show the real and imaginary parts of dielectric dispersion for the samples of CCTO_EW700 and CCTO_EW800 at various temperatures between -50 and -10 °C. It is clearly seen from Fig. 7a.1 and 7b.1 that both

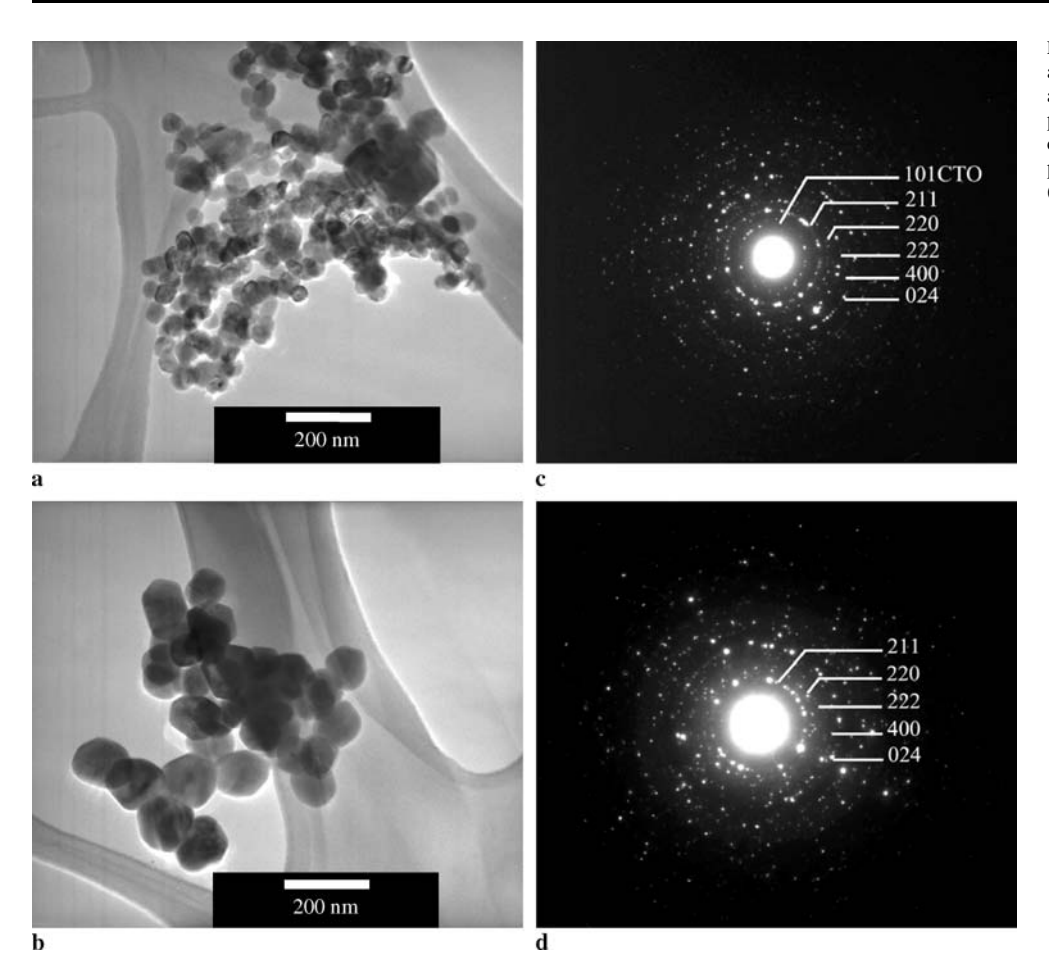


FIGURE 5 Bright field TEM images with corresponding selectedarea electron diffraction (SAED) pattern of CaCu₃Ti₄O₁₂ powders calcined in air for 8 h at different temperatures: (a) 700 °C and (b) 800 °C (CTO-CaTiO₃)

samples have very high dielectric constant, ε' , of $\sim 2.5 \times 10^4$ (at 1 kHz) for CCTO_EW700 and $\sim 1.5 \times 10^4$ (at 1 kHz) for CCTO_EW800. ε' has little frequency dependence at low frequency (below 100 kHz). Figure 8 compares the temperature dependence of the dielectric constant with the loss tangent at a frequency in the range of 100 Hz–1 MHz for the samples of CCTO_EW700 and CCTO_EW800. It is seen that the samples exhibits a giant dielectric constant, ε' , $\sim 5 \times 10^4$ (at 1 kHz) for CCTO_EW700 (Fig. 7c.1) and $\sim 4 \times 10^4$ (at 1 kHz) for CCTO_EW800 (Fig. 7d.1) at 150–190 °C with weak frequency dependence above 1 kHz. The values of tan δ of both samples (Fig. 7c.2 for CCTO_EW700 and Fig. 7d.2 for CCTO_EW800) are high and are in the range of ~ 0.2 –30 at temperatures between -50 and 190 °C. These tan δ values

Ring		rplanar spacing nples d_{hkl} (Å)	Standard (JCPDS: 7	
	700 °C powder	800 °C powder	$d_{hkl} (\mathring{\rm A})$	hkl
R_1	2.9719	2.9382	3.0173	211
R_2	2.5856	2.5456	2.6131	220
R_3	2.1021	2.1912	2.1336	222
R_4	1.8468	1.8469	1.8477	400
R_5	1.6789	1.6574	1.6526	024

TABLE 2 Measured interplanar spacings (d_{hkl}) obtained from selectedarea electron diffraction patterns of CCTO samples calcined at 700, and 800 °C for 8 h shown in Fig. 5. Corresponding values from the standard data JCPDS: 75-2188 are also provided for a comparison

increase with increasing temperature. The high ε' at low frequency may imply that there have grain boundary contributions in these sintered CCTO ceramics [44]. The values are similar to the those reported by Jin et al. [10] and Liu et al. [13] who reported values of $\varepsilon' \sim 10^4$ (at 1 kHz) for CCTO samples prepared from a solution route; and by Ramirez

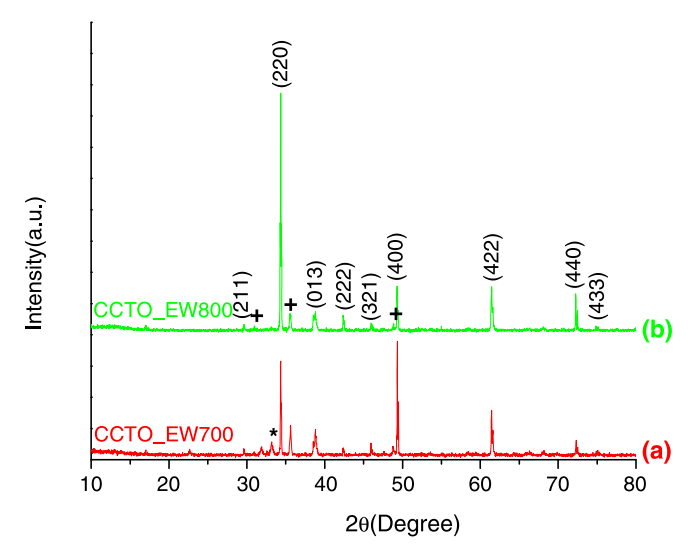


FIGURE 6 XRD patterns of (a) 700 °C; and (b) 800 °C, respectively. All sintering was done in air at 1100 °C for 16 h. The *indexed planes* indicated in all pattern are for CCTO main structure. (* – CaTiO₃ and + – CuO)

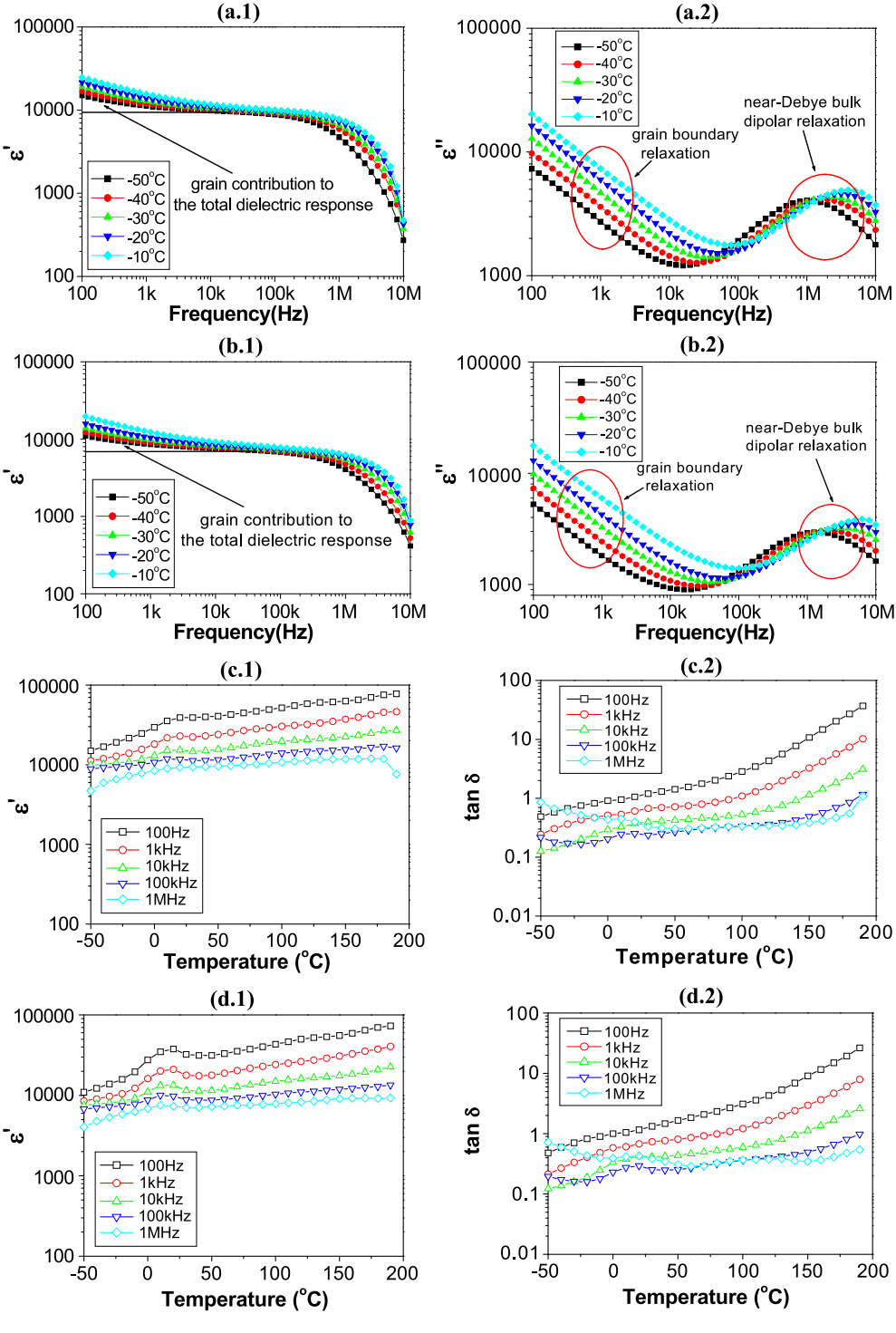


FIGURE 7 The frequency dependence of the complex permittivity, ε^* , at low temperature between -50 °C and -10 °C for CCTO_EW700 (a.1 and a.2) and CCTO_EW800 (b.1 and b.2), respectively. (a.1) and (b.1) display the real part ε' ; (a.2) and (b.2) display the imaginary part ε'' . The (c.1)-(d.1) and (c.2)-(d.2) show the temperature dependence of the dielectric constant, ε' , and $\tan \delta$ at frequency between 100 Hz and 1 MHz for CCTO_EW700 ($\mathbf{c.1}$ and $\mathbf{c.2}$) and CCTO_EW800 (d.1-d.2), respectively

Material	Grain size (µm)	Lattice parameter <i>a</i> (Å)	Activation energy of grains (eV)	Activation energy of grain boundaries (eV)
ASTM (75-2188)	-	7.391 ± 0.001	-	-
CCTO-EW700	12.0±7.8	7.388 ± 0.001	0.175	0.680
CCTO-EW800	15.5±8.9	7.393 ± 0.001	0.210	0.650

TABLE 3 Summary of grain size (from SEM), lattice parameter (from XRD), activation energy of grains (obtained from the curve fitting using (6)), and activation energy of grain boundaries (obtained from the curve fitting using (9)

et al. [1], and Bender and Pan [12], whose samples prepared from a solid state reaction method. These values, however, are much higher than $\sim 3\times 10^3$ of the polymeric citrate precursor routed CCTO ceramics reported by Jha et al. [8].

The imaginary parts of dielectric dispersion, ε'' are shown in Fig. 7a.2 and b.2 for the samples of CCTO_EW700 and CCTO_EW800, respectively. By considering these results, we cannot apply the empirical Cole–Cole relation to fit these

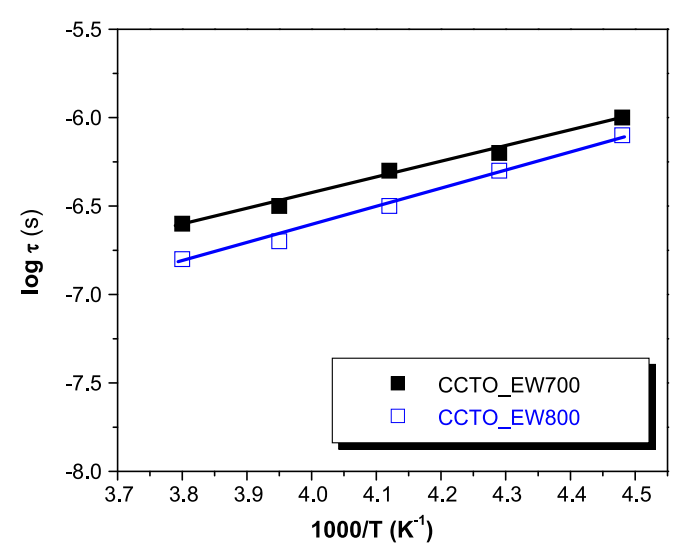


FIGURE 8 Arrhenius plot of the relaxation time for the sintered CCTO ceramics

data because the samples contain numerous grain boundaries or grain boundaries relaxation which was affected by low frequency [44]. However, we can apply the Debye-like relaxation model to these data since there are the relaxations contributed from the grains. The ε'' shows a clear Debye-like relaxation peak shifting from a constant value at low frequency to a small saturated value at higher frequency. The electrical response from the grains has a very high response frequency because of their small resistance and capacitance [13]. We can determine the dielectric relaxation time, τ , by following the Arrhenius law of

$$\tau = \tau_0 \exp\left(E_\tau/k_{\rm B}T\right) \,, \tag{6}$$

where τ_0 is the pre-exponential factor, E_{τ} is the activation energy for the relaxation, $k_{\rm B}$ is the Boltzmann constant, and T is the absolute temperature. The activation energy of an electrical response, at different temperature can be derived from the response time ($\tau=1/2\pi f$, where f is the response frequency at which the imaginary part of the complex impedance has a maximum). From the fitting shown in Fig. 8, we obtain the activation energy of the dielectric relaxation to be 0.175 eV for CCTO_EW700 and 0.210 eV for CCTO_EW800.

The ac conductivity, σ_{ac} , in most of the materials due to localized states may be described by [45]

$$\sigma_{\rm ac} = \sigma_{\rm dc} + A f^n \,, \tag{7}$$

where σ_{dc} is direct current conductivity. A, and n (0 < n < 1) are two temperature-dependent adjusting constants. From (7), the term of σ_{dc} presents the frequency independent part of the conductivity whereas the term of $A f^n$ is the frequency dependent part of the conductivity. However, our results did not fit well with (7) but the data can be fitted to equation

$$\sigma_{\rm ac} = \sigma_{\rm gb} + af^t + \alpha f^2 \,, \tag{8}$$

where $\sigma_{\rm gb}$ is the dc gain boundary conductivity, a, t and α are three adjustable constants [45]. In (8), the $\sigma_{\rm gb} + a f^t$ term describes the grain boundary conductivity relaxation [45].

The αf^2 term describes the transition between the two aforementioned relaxation behaviors [45,46]. Figure 9 shows the log-log plot of ac conductivity versus frequency of the CCTO ceramics at five different temperatures. The solid lines in Fig. 9a and b are the fitted results of (8) with t=0.53. For the CCTO_EW700, when the temperature increases from 150 °C to 190 °C, $\sigma_{\rm gb}$ and a increase from 3×10^{-6} to 1.5×10^{-5} S/cm and $9\times 10^{-8}-2.2\times 10^{-7}$ S/cm, respectively. For the CCTO_EW800, when the temperature increases from 150 °C to 190 °C, the values of $\sigma_{\rm gb}$ increases from $2\times 10^{-6}-9.5\times 10^{-6}$ S/cm, whereas the values of a rise from 7×10^{-8} to 2.2×10^{-7} S/cm. From the fitted results, we can obtain the dc gain boundary conductivity for the CCTO ceramics at different temperatures, and then we can fit $\sigma_{\rm gb}$ also by following the Arrhenius law of

$$\sigma_{\rm gb} = \sigma_{\rm gb}^0 \exp\left(-E_{\rm a}/k_{\rm B}T\right) , \qquad (9)$$

where $\sigma_{\rm gb}^0$ is the pre-exponential factor, $E_{\rm a}$ is the activation energy. From the fitting (Fig. 10), we obtain the activation energies of the dielectric relaxation for CCTO_EW700 and CCTO_EW800 to be 0.680 eV and 0.650 eV, respectively. These two values are comparable to the reported values of 0.60 eV [11] and 0.658–0.678 eV [18] for the grain bound-

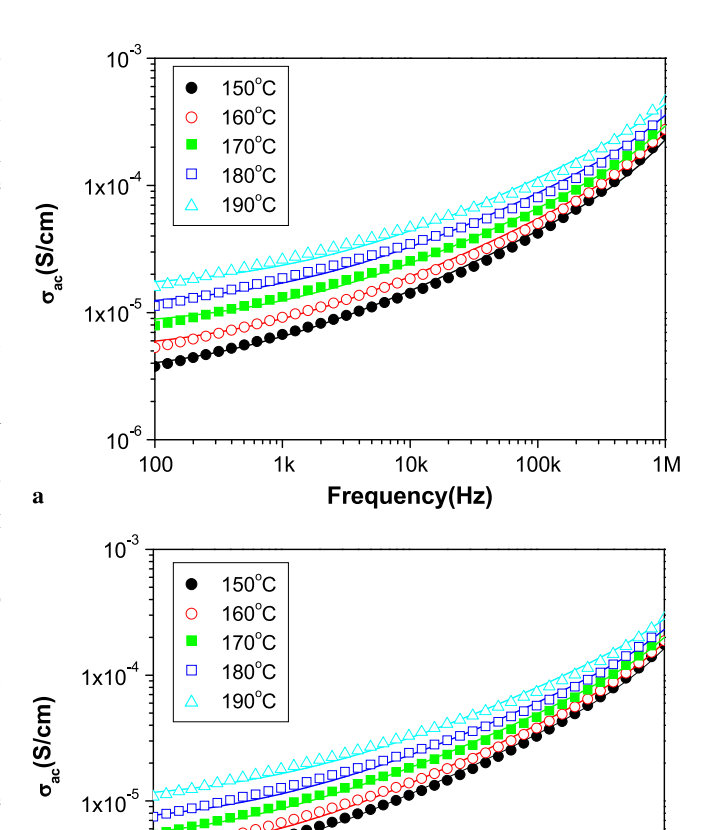


FIGURE 9 The frequency dependence of the ac conductivity, σ_{ac} , at high temperature ranging between 150 °C and 190 °C for (a) CCTO_EW700, and (b) CCTO_EW800, respectively. The *solid lines* are the fits according to (8)

1k

10k

Frequency(Hz)

100k

1M

10⁻⁶

100

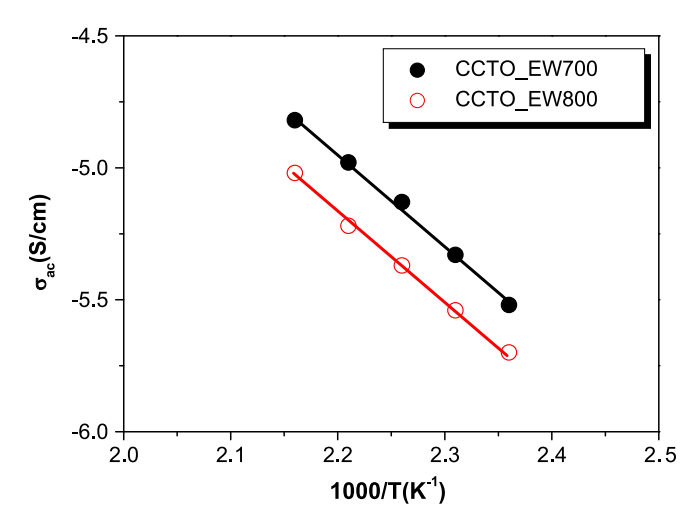


FIGURE 10 Arrhenius plot of ac conductivity, $\sigma_{\rm ac}$, for the sintered CCTO ceramics

aries of CCTO ceramics. As mentioned previously, we have shown that the all CCTO ceramics are electrically inhomogeneous. It consists of semi-conducting grains and insulating grain boundaries, which can be described by the hypothesis of the existence of internal barrier layers between the grains.

Since the dielectric response in both CCTO_EW700 and CCTO_EW800 shows the Debye-like relaxation which is approximately equal to the pure Debye functional form of a Maxwell–Wagner relaxation, the giant dielectric behavior of both samples can be explained by using Maxwell–Wagner relaxation model. The Maxwell–Wagner relaxation can be described by an equivalent circuit consisting of a series array of two sub-circuits, one representing grain effects and one grain boundaries [11, 13]. In each sub-circuit, the resistor and capacitor are in parallel. From this equivalent circuit, the static permittivity (ε_s') and dielectric relaxation time (τ) can be calculated as

$$\varepsilon_{\rm s}' = \left(R_{\rm g}^2 C_{\rm g} + R_{\rm gb}^2 C_{\rm gb} \right) / \left[C_0 \left(R_{\rm g} + R_{\rm gb} \right)^2 \right]$$
 (10)

and

$$\tau = \left[R_{\rm g} R_{\rm gb} \left(C_{\rm g} + C_{\rm gb} \right) \right] / \left(R_{\rm g} + R_{\rm gb} \right), \tag{11}$$

where $R_{\rm g}$, $R_{\rm gb}$ and $C_{\rm g}$, $C_{\rm gb}$ are the resistance and capacitance of grains and grain boundaries, respectively [47]. Since $R_{\rm gb} \gg R_{\rm g}$, and $C_{\rm gb}$ is also much larger than $C_{\rm g}$ [11, 13], the effective dielectric permittivity ($\varepsilon_{\rm s}'$) of the sample at frequencies much lower than the relaxation frequency $1/2\pi\tau$ can, therefore, be approximately from (10),

$$\varepsilon_{\rm s}' = C_{\rm gb}/C_0 \,. \tag{12}$$

Thus, ε_s' is determined by the ratio between grain boundary capacitance, $C_{\rm gb}$, and empty cell capacitance, C_0 . Hence ε_s' is constant when $C_{\rm gb}$ is temperature and frequency independent. The implication is in good agreement with our experimental results. We observed that dielectric constant is little dependent on the frequency and only weakly dependent on the temperature. And we can approximate τ from (11) using

$$\tau \approx R_{\rm g} C_{\rm gb} = \tau_{\rm g} (C_{\rm gb}/C_{\rm g}), \qquad (13)$$

where $\tau_g = R_g C_g$ is the response time of the grains [13]. It has been reported that C_g and C_{gb} are independent of temperature [11, 13], thus, we can deduce τ_g that follows the Arrhenius law, (6). Let $\tau_g = \tau_g^0 \exp(E_g/k_B T)$ (τ_g^0 is pre-exponential factor and E_g is the activation energy of the grain conduction process), then we modify (13) to

$$\tau \approx \frac{C_{\rm gb}}{C_{\rm g}} \tau_{\rm g}^0 \exp\left(E_{\rm g}/k_{\rm B}T\right). \tag{14}$$

Equation (14) shows that the activation energy of the dielectric process approximately equals that of the grain conduction process. On the basis of this analysis, we can conclude that the activation energy for the response of the grains in CCTO_EW700, and CCTO_EW800 to be 0.175 eV and 0.210 eV, which are lager than the value (0.08 eV) reported by Sinclair et at. using solid-state reaction [11].

From all the activation energy values, we have that the grain boundaries of all CCTO ceramics have a much larger activation energy (0.680 eV for CCTO_EW700 and 0.650 eV for CCTO_EW800) than that of the grains (0.175 eV for CCTO_EW700 and 0.210 eV for CCTO_EW800). This indicates that the all CCTO ceramics have a high energy barrier for the charge carriers to overcome. Therefore, the grain boundaries exhibit insulating properties. In contrast, the smaller activation energy of grains displays semiconducting properties similar to occur in other titanate-based materials [48].

At this time, the origin of semi-conducting grains and insulating grain boundaries has not been clearly established. Liu et al. [13] have proposed that the grains made by different method could have very different electrical property. Therefore, the larger activation energy of grains in CCTO_EW700 and CCTO_EW800 compared to that of a sample made by solid-state reaction implies that there are fewer oxygen vacancies in the grains of CCTO_EW700 and CCTO_EW800. This is reasonable because CCTO_EW700 and CCTO_EW800 were sintered from powders, which were calcined at low temperature (700 and 800 °C) compared to the temperature needed for the solid-state processing. However, it is premature to associate the increase in grain activation energy of all CCTO ceramics with its large dielectric constant.

4 Conclusions

CCTO nano-powders have been synthesized by simple egg white solution route. The synthesized powders were characterized by TG-DTA, XRD, FTIR, SEM, and TEM. The powders calcined at 700 and 800 °C were used to prepared bulk CCTO ceramics, which were sinterred at 1100 °C for 16 h. The dielectric behaviour of CCTO ceramics were obtained to similar to that of CCTO made by solid state reaction, i.e., there are a Debye-like relaxation in the samples and their giant dielectric constant are little dependent of frequency and temperature below the relaxation frequency. The dielectric properties of these CCTO ceramics are attributed to the Maxwell–Wagner polarization mechanism. This work demonstrates that a simple solution route using water-soluble egg white proteins can be used for preparation of giant dielectric CCTO ceramics. We believe that

the current simple, cost effective and environmental friendly synthesis method using water-soluble egg white proteins can be extended to prepare fine particles of other interesting materials.

ACKNOWLEDGEMENTS The authors would like to thank the Department of Chemistry, Khon Kaen University for providing TG-DTA, the Faculty of Science Electron Microscopy Unit, Khon Kaen University for providing SEM facilities and the Department of Materials Science and Engineering, the University of Arizona for providing TEM. C. Masingboon would like to thank the University Staff Development Program, Kasetsart University Chalermphrakiat Sakon Nakhon Province Campus, Thailand for financial support of his PhD study. This work is financially supported by the Thailand Research Fund (TRF).

REFERENCES

- 1 A.P. Ramirez, M.A. Subramanian, M. Gardel, G. Blumberg, D. Li, T. Vogt, S.M. Shapiro, Solid State Commun. 115, 217 (2000)
- 2 M.A. Subramanian, L. Dong, N. Duan, B.A. Reisner, A.W. Sleight, J. Solid State Chem. 151, 323 (2000)
- 3 C.C. Homes, T. Vogt, S.M. Shapiro, S. Wakimoto, A.P. Ramirez, Science 293, 73 (2001)
- 4 A.F.L. Almeida, R.S. de Oliveira, J.C. Góes, J.M. Sasaki, A.G. Souza Filho, J. Mendes Filho, A.S.B. Sombra, Mater. Sci. Eng. B **96**, 275 (2002)
- 5 M.A. Subramanian, A.W. Sleight, Solid State Sci. 4, 347 (2002)
- 6 Z. Yu, C. Ang, J. Appl. Phys. 91, 794 (2002)
- 7 L. Fang, M.R. Shen, Thin Solid Films 440, 60 (2003)
- 8 P. Jha, A.K. Arora Pand Ganguli, Mater. Lett. **57**, 2443 (2003)
- 9 J. Li, A.W. Sleight, M.A. Subramanian, Solid State Commun. 135, 260 (2005)
- 10 S. Jin, H. Xia, Y. Zhang, J. Guo, J. Xu, Mater. Lett. 61, 1404 (2007)
- 11 D.C. Sinclair, T.B. Adams, F.D. Morrison, A.R. West, Appl. Phys. Lett. 80, 2153 (2002)
- 12 B.A. Bender, M.J. Pan, Mater. Sci. Eng. B 117, 339 (2005)
- 13 J. Liu, Y. Sui, C. Duan, W.N. Mei, R.W. Smith, J.R. Hardy, Chem. Mater. 18, 3878 (2006)
- 14 P. Thongbai, C. Masingboon, S. Maensiri, T. Yamwong, S. Wongsaenmai, R. Yimnirun, J. Phys.: Condens. Matter 19, 236 208 (2007)
- S. Maensiri, P. Thongbai, T. Yamwong, Appl. Phys. Lett. 90, 202908 (2007)
- 16 S. Chung, I. Kim, S. Kang, Nat. Mater. 3, 774 (2006)
- 17 T.T. Fang, H.K. Shiau, J. Am. Ceram. Soc. 87, 2072 (2004)
- 18 S.F. Shao, J.L. Zhang, P. Zheng, W.L. Zhong, C.L. Wang, J. Appl. Phys. 99, 084106 (2006)

- 19 P. Lunkenheimer, V. Bobnar, A.V. Pronin, A.I. Ritus, A.A. Volkov, A. Loidl, Phys. Rev. B 66, 052 105 (2002)
- 20 P. Lunkenheimer, R. Fichtl, S.G. Ebbinghaus, A. Loidl, Phys. Rev. B 70, 172 102 (2004)
- 21 M.H. Cohen, J.B. Neaton, L.X. He, D. Vanderbilt, J. Appl. Phys. 94, 3299 (2003)
- 22 L. Zhang, Z.J. Tang, Phys. Rev. B 70, 174 306 (2004)
- 23 A.R. West, T.B. Adams, F.D. Morrison, D.C. Sinclair, J. Eur. Ceram. Soc. 24, 1439 (2004)
- 24 G. Chiodeli, V. Massarotti, D. Capsoni, M. Bini, C.B. Azzoni, M.C. Mozzati, P. Lupotto, Solid State Commun. 132, 241 (2004)
- 25 D. Capsoni, M. Bini, V. Massarotti, G. Chiodelli, M.C. Mozzatic, C.B. Azzoni, J. Solid State Chem. 177, 4494 (2004)
- 26 S.V. Kalinin, J. Shin, G.M. Veith, A.P. Baddorf, M.V. Lobanov, H. Runge, M. Greenblatt, Appl. Phys. Lett. 86, 102 902 (2005)
- 27 T.T. Fang, L.T. Mei, H.F. Ho, Acta Mater. 54, 2867 (2006)
- 28 B.L. Cushing, V.L. Kolesnichenko, C.J. O'Connor, Chem. Rev. 104, 3893 (2004)
- 29 D.V. Vadehra, K.R. Nath, CRC Crit. Rev. Food. Technol. 4, 193 (1973)
- 30 E. Li-Chen, S. Nakai, CRC Crit. Rev. Poultry Biol. 21 (1989)
- 31 Y. Mine, Trends Food Sci. Technol. 6, 225 (1995)
- 32 O. Lyckfeldt, J. Brandt, S. Lesca, J. Eur. Ceram. Soc. 20, 2551 (2000)
- 33 S. Dhara, P. Bhargava, J. Am. Ceram. Soc. 84, 3045 (2001)
- 34 S. Dhara, P. Bhargava, J. Am. Ceram. Soc. 86, 1645 (2003)
- 35 S. Dhara, J. Am. Ceram. Soc. 88, 2003 (2005)
- 36 S. Maensiri, C. Masingboon, P. Laokul, W. Jareonboon, V. Promarak, P.L. Anderson, S. Seraphin, Cryst. Growth Design 7, 950 (2007)
- 37 S. Maensiri, C. Masingboon, B. Boonchom, S. Seraphin, Scripta Mater. 56, 797 (2006)
- 38 W. Li, R.W. Schwartz, Appl. Phys. Lett. 89, 242 906 (2006)
- 39 S. Guillemet-Fritsch, T. Lebey, M. Boulos, B. Durand, J. Eur. Ceram. Soc. 26, 1245 (2006)
- 40 B.D. Cullity, S.R. Stock, *Elements of X-ray Diffraction* (Prentice Hall, Upper Saddle River, 2001)
- 41 C.L. Kretly, A.F.L. Almeida, P.B.A. Fechine, R.S. De Oliveira, A.S.B. Sombra, J. Mater. Sci. Mater. Electron. 15, 657 (2004)
- 42 P. Leret, J.F. Fernandez, J. de Frutos, D. Fernández-Hevia, J. Eur. Ceram. Soc. 27, 3901 (2007)
- 43 C.K. Yeoh, M.F. Ahmad, Z.A. Ahmad, J. Alloys Compd. 443, 155 (2007)
- 44 M.A. Ramirez, P.R. Bueno, J.A. Varela, E. Longo, Appl. Phys. Lett. 89, 212 102 (2006)
- 45 L. Zhang, Appl. Phys. Lett. 87, 022 907 (2005)
- 46 S. Capaccioli, M. Lucchesi, P.A. Rolla, G. Ruggeri, J. Phys.: Condens. Matter 10, 5595 (1998)
- 47 V. Hippel, Dielectrics and Waves (Wiley, New York, 1954)
- 48 F.D. Morrison, D.C. Sinclair, A.R. West, J. Am. Ceram. Soc. 84, 474 (2001)



Available online at www.sciencedirect.com



Scripta Materialia 60 (2009) 870-873



www.elsevier.com/locate/scriptamat

Giant dielectric response and polarization relaxation mechanism in (Li,V)-doped NiO ceramics

Sarawut Pongha, a Prasit Thongbai, Teerapon Yamwong and Santi Maensiria, *

^aSmall & Strong Materials Group (SSMG), Department of Physics, Faculty of Science, Khon Kaen University, Khon Kaen 40002, Thailand

^bNational Metals and Materials Technology Center (MTEC), Thailand Science Park, Pathumthani 12120, Thailand

Received 11 November 2008; revised 28 January 2009; accepted 29 January 2009 Available online 5 February 2009

We report the giant dielectric response in (Li,V)-doped NiO ($\text{Li}_{0.05}\text{V}_{0.02}\text{Ni}_{0.93}\text{O}$, $\text{Li}_{0.05}\text{V}_{0.05}\text{Ni}_{0.90}$ and $\text{Li}_{0.05}\text{V}_{0.10}\text{Ni}_{0.85}\text{O}$) ceramics. Microstructure and phase composition analyses reveal that the ceramics consist of a core/shell structure that is rich in V dopant at the grain boundary. The dielectric response and related electrical properties of these materials are strongly affected by the V content. The giant dielectric behavior of the LVNO ceramics is mainly attributed to the Maxwell–Wagner polarization and thermally activated mechanisms.

© 2009 Acta Materialia Inc. Published by Elsevier Ltd. All rights reserved.

Keywords: Ceramics; Dielectrics; Dielectric properties; Electrical properties; Grain boundaries

High-permittivity dielectric materials with good thermal stability and free of Ba and Pb have been used for some time as important elements in capacitors and memory devices, and have hence played a significant role in microelectronics. In recent years there has been intensive research into new high dielectric materials because these might offer the opportunity to increase the choice of materials for various practical applications. High-permittivity NiO-based ceramics, non-perovskite and non-ferroelectric materials with the formula $A_x B_y \text{Ni}_{1-x-y} \text{O}$ (where A = monovalents of Li, Na, K and B = Ti, Al, Ta, Si) [1–7], have attracted considerable attention in recent years due to their impressive high apparent dielectric permittivity (ε') of 10^3-10^5 , which remains constant over the temperature range from -50 to 150 °C [1.5]. Moreover, the dielectric properties of such material systems can be tuned by varying the composition via additions of A and B[1]. However, an explanation of this high dielectric permittivity is still unclear and incomplete. Therefore, it is important to search for the new giant dielectric materials in NiO-based ceramic systems and attempt to clarify the origin of the giant

dielectric permittivity and the polarization relaxation behavior of these ceramics.

In this paper, we investigate the dielectric properties of polycrystalline $\text{Li}_{0.05}\text{V}_x\text{Ni}_{0.95-x}\text{O}$ (LVNO) ceramics. These materials exhibit giant ε' values of $3\text{--}6\times10^4$, which decrease with increasing V content. The observed core/shell structure in the LVNO ceramics may be responsible for this apparent giant ε' . Our results reveal that the activation energy required for relaxation and the related conduction activation energy in the grain interiors increases with increasing V concentration, and both of these activation energies are almost the same in value. The giant ε' behavior of this system is mainly attributed to the Maxwell–Wagner relaxation and thermally activated mechanisms.

In this work, Ni(NO₃)₂·6H₂O, LiNO₃, C₁₀H₁₄O₅V, (NH₄)₂S₂O₈ and acrylic acid were employed as starting raw materials. The polycrystalline LVNO ceramic samples with different additions of V, i.e. Li_{0.05}V_{0.02}Ni_{0.93}O (LVNO-02), Li_{0.05}V_{0.05}Ni_{0.90}O (LVNO-05) and Li_{0.05}V_{0.10}Ni_{0.85}O (LVNO-10), were designed and prepared by the following procedure. Firstly, stoichiometric amounts of Ni(NO₃)₂·6H₂O, C₁₀H₁₄O₅V and LiNO₃ were dissolved in 10 g of acrylic acid aqueous solution (acrylic acid:H₂O = 70:30 wt.%) under constant stirring and heating at 100 °C. Secondly, a small amount (0.5 g) of 5% (NH₄)₂S₂O₈ aqueous solution as the initiator was added to the mixed acrylic acid solution

^{*} Corresponding author. Tel.: +66 43 202222-9x2248; fax: +66 43 202374; e-mail addresses: sanmae@kku.ac.th; santimaensiri@gmail.com

to promote the polymerization. Then, the gel precursors were dried at 350 °C for 1 h. To obtain the LVNO powders, the dried gels were ground and later calcined at 700 °C for 5 h in air. The LVNO powders were pressed into pellets 9.5 mm in diameter and $\sim 1-2$ mm in thickness by a uniaxial pressing method at 200 MPa. Finally, these pellets were sintered at 1280 °C for 4 h in air.

X-ray diffraction (XRD) (Philips PW3040, The Netherlands) and scanning electron microscopy (SEM) (Hitachi S-4700) coupled with energy-dispersive X-ray spectrometry (EDS) were used to characterize the phase composition and microstructure of the LVNO ceramics. The sintered ceramic samples were polished and electroded by silver paint on both sides of the disk-shaped samples. The dielectric and electrical responses of the samples was measured using a Hewlett–Packard 4194A impedance gain phase analyzer over the frequency range from 100 Hz to 10 MHz and at an oscillation voltage of 1.0 V. The measurements were performed over the temperature range from -50 to $100\,^{\circ}\text{C}$ using an inbuilt cooling–heating system. Each measured temperature was kept constant with an accuracy of $\pm 1~\text{K}$.

Figure 1a–c shows the XRD patterns of the LVNO powders and the as-sintered ceramic samples with different V-doped contents, confirming a main phase of NiO in all the samples. The second phase of Ni₃V₂O₈ was only observed in the LVNO powder samples, but was not detected in the as-sintered LVNO samples. However, after the as-LVNO-10 sample was polished, the second phase of Ni₃V₂O₈ could be observed (Fig. 1d). This might be due to the outermost layer surface of the sintered samples being V-phase deficient. A similar observation has been reported for CaCu₃Ti₄O₁₂ (CCTO)/Ag composites that are Ag deficient in the outermost layer and Ag rich in the inner part [8]. SEM-EDS measurements (the upper inset of Fig. 1) of the grain and grain boundary (GB), however, show that the GB is rich in V dopant that has been lost from the grain. Therefore, our LVNO samples have a heterogeneous core/shell structure containing Li-doped NiO

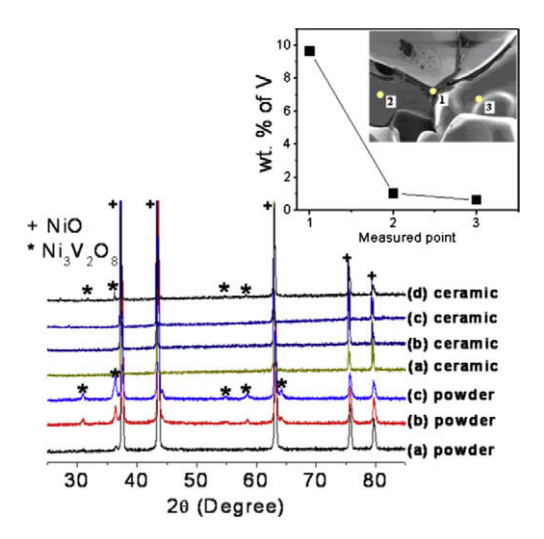


Figure 1. XRD patterns of the LVNO powders and sintered LVNO ceramics: (a) LVNO-02 sample; (b) LVNO-05 sample; (c) LVNO-10 sample; and (d) XRD pattern of LVNO-10 with polished surface. Inset shows the element profile obtained from EDS spectra.

particles and insulating V-rich boundary layer (i.e. $Ni_3V_2O_8$), respectively.

The dielectric properties of the LVNO samples were measured over wide ranges of temperature and frequency. The ε' values at 1 kHz and room temperature for the LVNO-02, LVNO-05 and LVNO-10 samples are 61,907, 34,854, and 30,503, respectively. All the LVNO samples exhibit high ε' values. ε' decreases with increasing V concentration, which can be attributed to the increase in the thickness of the GB layer $(t_{\rm gb})$. A similar result has been reported for $Li_xTi_vNi_{1-x-v}O$ (LTNO) system, and the giant ε' of this LTNO system was explained by a simple series-layer model for the boundary-layer capacitors (BLCs) [1]. Figure 2 demonstrates the frequency dependence of the dielectric permittivity (ε') and dielectric loss (ε'') of the LVNO-05 sample at different temperatures. ε' shows high values at low frequencies, and rapidly decreases if the frequency is sufficiently high. This step decrease shifts to higher frequency with increasing temperature, corresponding to the movement of the ε'' peaks. This behavior is similar to that observed in other NiO-based ceramic systems [1,3-5] and the other giant dielectric systems such as CCTO [9,10] and CuO ceramics [11,12]. Such behavior is typical for the Maxwell-Wagner relaxation, which is generally employed to describe the observed high ε' in electrically inhomogeneous materials [13]. Thus, the observed core/shell structure in our LVNO samples is responsible for their apparent giant ε' .

Usually, the dielectric relaxation behavior provides important clues to explain the related mechanism in materials [14]. Therefore, we plotted $\ln(\tau)$ vs. 1/T in the inset of Figure 2, in which the solid lines are the fitted results obeying the Arrhenius law, i.e.

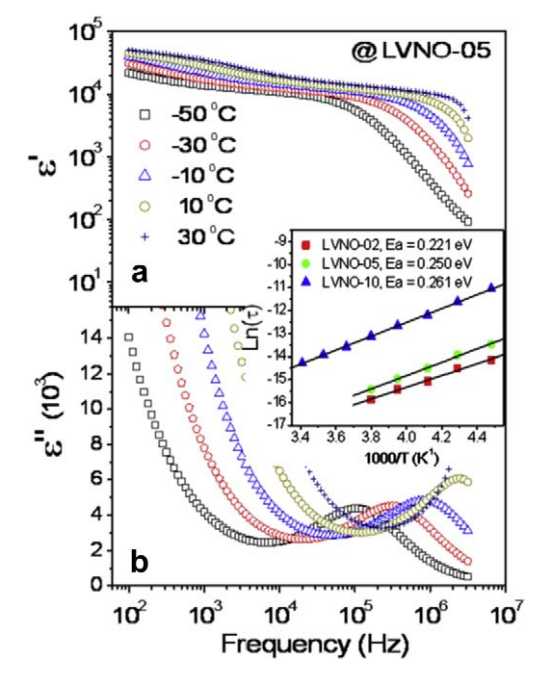


Figure 2. Frequency dependence of (a) the dielectric permittivity (ε') and (b) dielectric loss (ε'') at different temperatures. Inset is the temperature dependence of the relaxation time for the different LVNO samples; the solid lines are fitted to experimental results by using Eq. (1).

$$\tau = \tau_0 \exp(E_a/k_B T),\tag{1}$$

where τ_0 is the pre-exponential factor, $E_{\rm a}$ is the relaxation activation energy, $k_{\rm B}$ is the Boltzmann constant, and T is the absolute temperature. τ is calculated from the relations $\omega \tau = 1$ and $\omega = 2\pi f_{\rm p}$, where $f_{\rm p}$ is the frequency at the peak of ε'' as displayed in Figure 2b. According to the fitted curve in the inset of Figure 2 for the LVNO samples with different V contents, $E_{\rm a}$ values of 0.221, 0.250, and 0.261 eV can be obtained for the samples of LVNO-02, LVNO-05 and LVNO-10, respectively.

To characterize the electrical properties of the core/ shell structure in the LVNO ceramics, impedance spectroscopy (IS) [15], which is a powerful tool to separating out the bulk and the GBs effects, was carried out. As illustrated in Figure 3a, the impedance semicircle spectra of the LVNO-10 sample become larger with decreasing temperature. When the temperature is sufficiently low, other impedance semicircles can be observed (inset of Fig. 3a). The observation of the two semicircles suggests that our LVNO ceramics are electrically heterogeneous, and thus a core/shell model is used for further analysis. Accordingly, the observed semicircles at higher and lower temperatures can be assigned to the effects of charge transport within the grain and GB, respectively. Note that the impedance spectra of the LVNO-02 and LVNO-05 samples are similar to that of the LVNO-10 sample, but their impedance semicircles at low temperature cannot be detected (are not present). This might be attributed to the electrical responses of the grain of these samples being shifted out of the measured frequency

As is known, the conduction mechanism of the Li-doped NiO system can be well explained by the polaron hopping

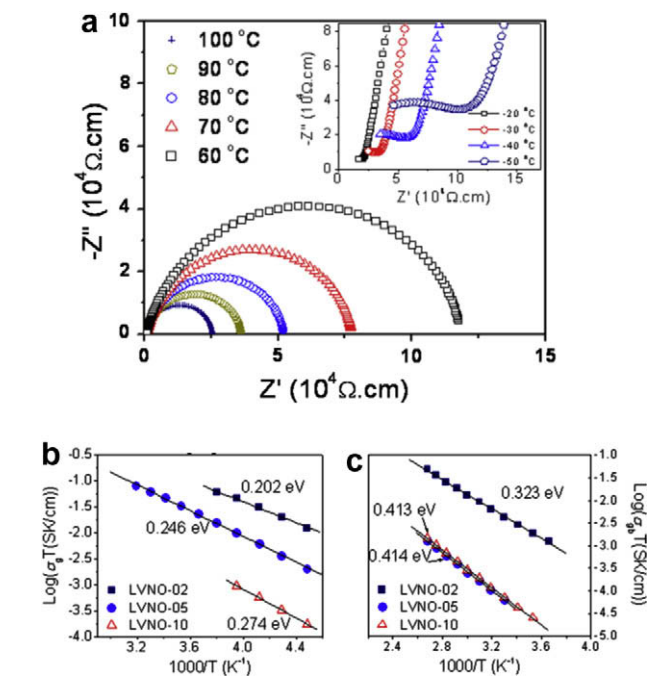


Figure 3. (a) Impedance spectra as a function of temperature for the LVNO-10 sample. (b and c) Arrhenius plots of the grain and GB conduction of the LVNO samples.

theory [4,13]. In polaronic scenario, the temperature dependence of the conductivity (σ) has a temperature-dependent prefactor, described by [13]:

$$\sigma \propto T^{-1} \exp(-E/k_{\rm B}T),$$
 (2)

where E is the conduction activation energy. Normally, the GB effect on electric conductivity may originate from a GB potential barrier [13], which can be ascribed to the V-rich boundary for the LVNO system. From the intercepts of each semicircular arc with the real axis, the resistance of the grain ($R_{\rm g}$) and the resistance of the GB ($R_{\rm gb}$) can be calculated. As a result, conductivity data were obtained for the grain ($\sigma_{\rm g}$) and GB ($\sigma_{\rm gb}$) components. Interestingly, the temperature dependence of $\sigma_{\rm g}$ and $\sigma_{\rm gb}$ follows Eq. (2) as shown in Figure 3b and c, respectively. As a result, the conduction activation energies inside the grain ($E_{\rm g}$) and at the GB ($E_{\rm gb}$) can be obtained-the values of $E_{\rm g}$ are 0.202, 0.246 and 0.274 eV, while the values of $E_{\rm gb}$ are 0.323, 0.414 and 0.413 eV for the samples of LVNO-02, LVNO-05 and LVNO-10, respectively. These results strongly indicate that the grain and GB have different characteristics of electrical transport.

It is important to note that the values of E_g and E_a of each sample are almost the same in value. A similar result was observed in the LTNO system as reported by Lin et al. [13]. The authors explained that the natures of the charge carriers responsible for dielectric relaxation peaks and DC conduction belonged to the same category, which indicated that the polarization relaxation was closely related to the conductivity in the grain interior, and the polarization process depended on the conductance of charge in the grain interior. Moreover, it is interesting that both E_g and E_a in our LVNO samples increase with increasing \tilde{V} content, but E_{gb} changes only slightly when the V-dopant level is more than 5 mol.%. These results suggest that the $Ni_3V_2O_8$ phase only changes the t_{gb} value, which has an influence on the ε' value, but not the intrinsic properties of the LVNO ceramics. Furthermore, it can be seen that the concentration of the V dopant has a strong effect on the electrical transport characteristic inside the grain and the related dielectric behavior of the LVNO ceramics. This is due to the fact that some V atoms have entered into the NiO crystal lattice (indicated by the EDS analysis in the inset of Figure 1), leading to the variation in E_g . Obviously, the LVNO-02 sample with the smaller $E_{\mathfrak{g}}$ value shows the highest ε' value of these three samples. This is possibly due to the following two reasons. First, the polarization process is closely related to the conduction of charge carriers in the grain interior [16]; second, the $t_{\rm gb}$ of the LVNO-02 sample is smaller than those of the other two samples [1]. Additionally, we found that the temperature at the loss peak at the fixed frequency shifts to lower temperature with decreasing V concentration (not shown), corresponding to the decrease in $E_{\rm g}$. This is because the electrical charge carriers in the grain interiors of the sample with the lowest $E_{\rm g}$ can easily be thermally activated. Therefore, the discrepancy in E_g and t_{gb} of each sample caused by the different concentrations of V doping results in the various dielectric behavior observed in the LVNO system.

It is important to note that the loss tangents $(\tan \delta)$ of these LVNO ceramics are still too high, i.e. $\tan \delta \sim 13.06$,

1.13 and 1.34 (at room temperature and 1 kHz) for the samples of LVNO-02, LVNO-05 and LVNO-10, respectively. The high loss is undesirable for practical applications. Normally, it is believed that the strategy to reduce the dielectric loss is to increase the resistance of GB [17]. This is reasonable for giant-permittivity core/shell materials because the charges in the semiconducting core grains are restricted by the insulating GBs, under an electric field. However, $\tan \delta$ shows a small change when the V concentration increases from 5 up to 10 mol.%, and thus we believe that $\tan \delta$ in the LVNO ceramics cannot be decreased by increasing the V concentration due to the intrinsic properties of Ni₃V₂O₈ phase. It will be very important to look for suitable new **B**-dopants of $A_x B_{y-}$ $Ni_{1-x-y}O$ which can modify the defect equilibrium at GBs, leading to the higher resistance of GBs.

In conclusion, the giant dielectric permittivity, ε' , and related electrical properties of LVNO ceramics have been characterized as functions of frequency and temperature. EDS results reveal that the structure is rich in V dopant at the GB, and contains an insulating Ni₃V₂O₈ phase. The concentration of V has a remarkable effect on the dielectric properties of the LVNO ceramics due to the difference in the values of E_g and t_{gb} . The giant ε' behavior of the LVNO ceramics can be explained based on the Maxwell–Wagner polarization (i.e. interfacial polarization) and thermally activated mechanisms.

The authors would like to thank the Department of Physics, Ubon Ratchathani University and the Thai Microelectronics Center for providing XRD and FE-SEM facilities, respectively. S.P. and P.T. would like to thank The National Science and Technology Development Agency for financial support of their studies through the YSTP and TGIST Programs, respectively. This work was financially supported by the Thailand Research Fund and the Commission on Higher Education, Thailand.

- [1] J. Wu, C.W. Nan, Y.H. Lin, Y. Deng, Phys. Rev. Lett. 89 (2000) 217601.
- [2] S. Maensiri, P. Thongbai, T. Yamwong, Acta Mater. 55 (2007) 2851.
- [3] Y.H. Lin, J. Wang, L. Jiang, Y. Chen, C.W. Nan, Appl. Phys. Lett. 85 (2004) 5664.
- [4] Y.H. Lin, L. Jiang, R. Zhao, C.W. Nan, Phys. Rev. B 72 (2005) 014103.
- [5] P.K. Jana, S. Sarkar, B.K. Chaudhuri, Appl. Phys. Lett. 88 (2006) 182901.
- [6] P.K. Jana, S. Sarkar, H. Sakata, T. Watanabe, B.K. Chaudhuri, J. Phys. D 41 (2008) 065403.
- [7] Y.J. Hsiao, Y.S. Change, T.H. Fang, T.L. Chai, C.Y. Chung, Y.H. Chang, J. Phys. D 40 (2007) 863.
- [8] C.C. Wang, Y.J. Yan, L.W. Zhang, M.Y. Cui, G.L. Xie, B.S. Cao, Scripta Mater. 54 (2006) 1501.
- [9] C.C. Homes, T. Vogt, S.M. Shapiro, S. Wakimoto, A.P. Ramirez, Science 293 (2001) 673.
- [10] P. Thongbai, C. Masingboon, S. Maensiri, T. Yamwong, S. Wongsaenmai, R. Yimnirun, J. Phys: Condens. Matter 19 (2007) 236208.
- [11] S. Sarkar, P.K. Jana, B.K. Chaudhuri, H. Sakata, Appl. Phys. Lett. 89 (2006) 212905.
- [12] P. Thongbai, S. Maensiri, T. Yamwong, J. Appl. Phys. 104 (2008) 036107.
- [13] Y.H. Lin, M. Li, C.W. Nan, J. Li, J. Wu, J. He, Appl. Phys. Lett. 89 (2006) 032907.
- [14] J. RossMacdonald, Impedance Spectroscopy, Wiley, New York, 1987.
- [15] D.C. Sinclair, T.B. Adams, F.D. Morrison, A.R. West, Appl. Phys. Lett. 80 (2002) 2153.
- [16] B. Cheng, Y.H. Lin, A. Mei, J.N. Cai, C.W. Nan, J. He, Appl. Phys. Lett. 92 (2008) 142903.
- [17] E.A. Patterson, S. Kwon, C.C. Huang, D.P. Cann, Appl. Phys. Lett. 87 (2005) 182911.

SIAM PHYSICS CONGRESS 2010

Physics for Creative Society

Kanchanaburi, THAILAND, March 25-27, 2010

ABSTRACTS



Organized by



















MP O2

Giant Dielectric Behavior of LixTipNi1-x-yO Ceramics

P. Thongbai ^{1*}, T. Yamwong² and S. Maensiri¹

Department of Physics, Faculty of Science, Khon Kaen University,

Khon Kaen, Thailand

National Metals and Materials Technology Center (MTEC), Thailand Science

Park, Pathumthani 12120, Thailand

Abstract

Giant dielectric properties of Li_xTi_yNi_{1-x-y}O ceramics were investigated as functions of temperature, frequency, and dc bias. Our results revealed that the concentrations of Li and Ti doping ions had a remarkable influence on the microstructure and the dielectric properties of the Li_xTi_yNi_{1-x-y}O ceramics. Interestingly, two thermally activated dielectric relaxations were detected in the dielectric spectra of the Li_xTi_yNi_{1-x-y}O ceramics, suggesting that there were at least two sources of polarization contributing to the total dielectric response in the Li_xTi_yNi_{1-x-y}O ceramics. It was also suggested that the surface treatment had an impact on the dielectric behavior of the Li_xTi_yNi_{1-x-y}O ceramics. The observed giant dielectric properties of the Li_xTi_yNi_{1-x-y}O ceramics might be attributed to an internal barrier layer capacitance effect based on the Maxwell-Wagner polarization or/and the small polaron hopping inside the grains.

Keyword: Dielectric loss and relaxation, Electrical properties

Corresponding author. Email: prasitphysics@hotmail.com

	[IM_O3]	Joint DC Resistivity and Audio Magnetotelluric Inversion: a Technique for Audio Magnetotelluric Static Shift Removal Puwis Amatyakul Mahidol University, Thailand	70
ral Presenta	tion : Ion and Plasma F	thysics	
	[IP_O1]	Development of Compact Helicon Plasma Source Generating at Very High Radio Frequency Pansak Kerdtongmee Walailak University, Thailand	71
	[IP_O2]	Plasma Dynamics Simulation in Small Theta Pinch Device Sidthisak Chaisombat Chulalongkorn University, Thailand	72
	[IP_O3]	Simple Estimation of Degree of Cross-linking in Tapioca Starch Induced by Atmospheric Argon Plasma Somsak Dangtip Mahidol University, Thailand	73
	[IP_O4]	FTIR Study of Effects of Atmospheric Argon Plasma On Tapioca Starch Panakamol Deevai Mahidol University, Thailand	74
	[IP_O5]	Predictions of ISTTOK Plasma Behaviors Using BALDUR and TASK Codes Nopporn Poolvarat Thammasat University, Thailand	75
	[IP_O6]	Prediction of Density and Temperature in L-mode Tokamak Plasmas <u>Apichart Siriwitpreecha</u> King Mongkut's University of Technology North Bangkok, Thailand	76
	[IP_O7]	Analysis of Internal Transport Barrier in <i>H</i> -Mode Plasmas and Development of Toroidal Velocity Models Boonvarit Chatthong Mahidol University, Thailand	77
	[IP_O8]	Behaviours of Impurity in ITER Plasma with Standard Type I ELMy H-Mode Scenario Chinda Chuchinda Thammasat University, Thailand	.78
	[IP_O9]	New Models for Predicting Pedestal Temperature and Density in ELMy H-Mode Plasma Wannapa Buangam Mahidol University, Thailand	79
Oral Presenta	ntion : Material physics		
	[MP_O1]	New High efficient Luminescent Materials for LED Application Mihail Nazarov Gwangju Institute of Science and Technology, Republic of Korea	80
	[MP_O2]	Giant Dielectric Behavior of Li ₄ Ti ₃ Ni ₃₋₄₊ O Ceramics <u>Prasit Thongbai</u> Khon Kaen University, Thailand	81
	[MP_O3]	Electromagnetic Properties of Material Characterization at Microwave Frequency Surivun Pongvitsakul IRC Technologies Limited, Thailand	82
	[MP_O4]	The Effect of Copper Addition on β-FeSi ₂ Synthesis Somehai Klatgamolehai Chulalongkom University, Thailand	83

International Conference on Smart Materials Smart/Intelligent Materials and Nanotechnology

2nd International Workshop on **Functional Materials and Nanomaterials**

Smartmat-'08 & IWOFM-2

> 22-25 April 2008 Chiang Mai, Thailand

Supported by





















	Room 5					Poster	Session		(8)
	Room 4					Specialty Polymers with Controlled Microstructures I Session Chair: Pitt Supaphol	Defining structure in electrospun polymer fibres (INVITED) Geoffrey Mitchell, University of Reading, U. K.	MO0020: Morphology of Electrospun Mats of Soy Protein Isolate and its Blend M. Phiriyawirut, N. Rodchanacheewa, N. Nensiri, P. Supaphol	MO00477: Fabrication of Patterned SU-8 Micromold Stamp for Low Cost Hot Embossing T. Lomas, S. Mongpranect, A. Sapphat, A. Wisitsora-at, A. Tuantranont
24 April 2008 (Continue)	Room 3 (IWOFM-2)	Nano-materials as Electrode for Li Ion Batteries (INVITED) B.V.R. Chowdhari, National University of Singapore (NUS), Singapore		1000459: Vertical-aligned ZnO nanorods only by radio frequency magnetron sputter Chuan-Pu Liu, Jun-Hang Huang	ch	Nano Materials/Structures II Session Chair: Tadashi Takenaka,	Hydrothermal Synthesis of ZnO rods, films, and 3-D structures at 90 °C (INVITED) Jin Hyeok Kim, Chonnam National University, Korea	Magnetic nanoparticles as smart heating mediator for hyperthermia and sorbent regeneration (INVITED) Nguyen Xuan Phuc, Institute of Materials Science (IMS), Vietnam	
24 Apr	Room 2	JO00449: Structural, Magnetic and Electrical Properties of SiO ₂ Added Strontium Hexa-ferrites M. Anis-ur-Rehman, G. Asghar			Lunch	MEMS/NEMS Session Chair: Preecha Yupapin.	Laser Molecular Beam Epitaxy and Multi-functional Thin Films (INVITED) Zhu Weiguang, Nanyang Technological University, Singapore	NO00155: High Resolution X-ray Diffraction and Raman Scattering Studies of Cubic-Phase InN Films Grown by MBE S. Kuntharin, S. Sanorpim, Y. Iwahashi, H. Yaguchi, A. Nishimoto, M. Orihara, Y. Hijakata, S. Yoshida	NO00465: InGaPN/CaP Lattice- matched Single Quantum Wells on GaP (001) Grown by MOVPE D. Kaewket, S. Sanorpim, S. Tungasmita, R. Katayama, K. Onabe
	Room 1	AO00072: Sonocatalyzed Ammonothermal Preparation of Fine Lithium Niobate Powders A. Rujiwatra, N. Thammajak, Y. Chimupala, P. Laoratanakul				Smart Materials/Systems Session Chair: R.P. Tandon	Phase Transitions and Dielectric Properties in Bi(Zn ₁₀ Ti ₁₀ O ₃ -ABO ₃ Perovskite Solid Solutions (INVITED) David P. Cann, Oregon State University, USA	NO00448: Sintering Effects and Oxygen Vacancies Roles on the Dielectric Properties of CaCu ₃ Ti ₄ O ₁₂ Ceramics C. Maxingboon, T. Yamwong, S. Maensiri	NO00472: High Dielectric Response in (Li, Ti)-doped NiO Ceramics Prepared by A Simple Thermal Decomposition Method P. Thongbai, T. Yamwong, S. Maensiri
Date/Time		11,15-11,30	11.30-11.45	11.45-12.00	12.00-13.00		13.00-13.30	13.30-13.45	13.45-14.00



High Dielectric Response in (Li, Ti)-doped NiO Ceramics Prepared by a Simple Thermal Decomposition Method

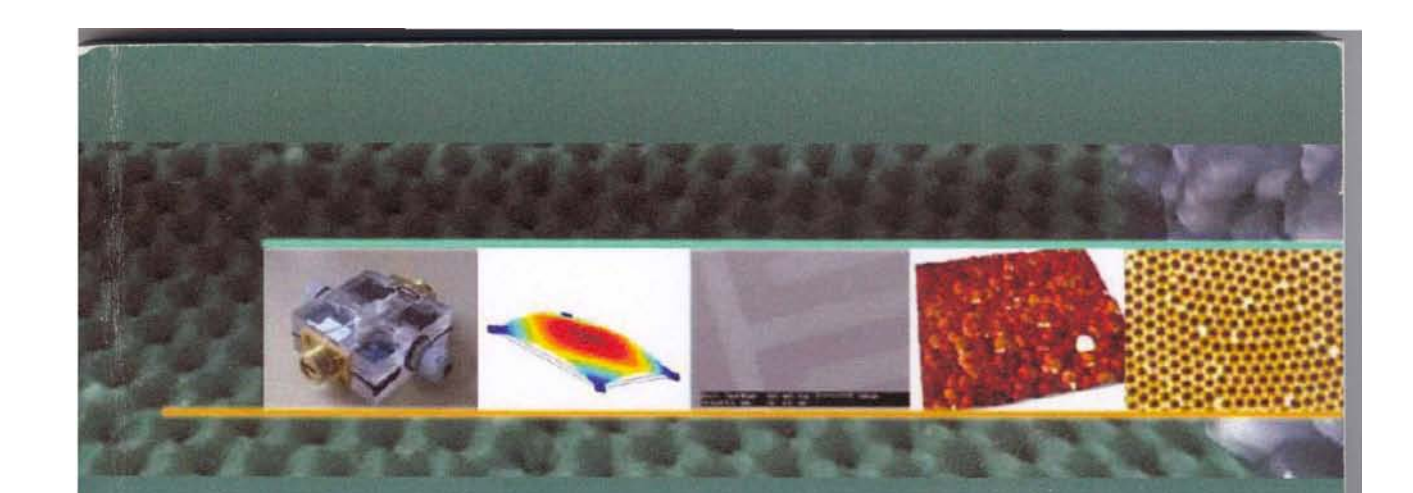
P. Thongbair, T. Yamwong2 and S. Maensiri1,3

¹ Small & Strong Materials Group (SSMG), Department of Physic, Faculty of Science, Khon Kaen University, Khon Kaen, 40002, Thailand

² National Metals and Materials Technology Center (MTEC), Thailand Science Park, Pathumthani, 12120, Thailand Integrated Nanotechnology Research Center (INRC), Faculty of Science, Khon Kaen University, Khon Kaen, 40002, Theiland

* Corresponding author : prasitphysics@hotmail.com

High dielectric permittivity (Li, Ti)-doped NiO (LTNO) (i.e. Li Ti Ni) $_{1-xy}^{1}$ O) ceramics were prepared by a simple thermal decomposition method. Structure and microstructure of the sintered samples were studied by XRD and SEM, respectively. The dielectric properties were investigated at temperature in the range of 223-473 K over various frequencies (10^2 - 10^6 Hz). The sintered LTNO samples exhibited high dielectric properties, and the dielectric constant reached about 10^4 at room temperature and 100 Hz for LTNO ceramics. The dielectric permittivity increases with increasing Li concentration and it decreases be a sint of the dielectric permittivity increases with increasing Li concentration and it decreases that the grain and grain boundary have also remarkable influence on dielectric properties due to the various activation energies corresponding to the dielectric relaxation processes. The high dielectric permittivity response of the LTNO ceramics is mainly enhanced by Maxwell-Wagner bigh dielectric permittivity response of the LTNO ceramics is mainly enhanced by Maxwell-Wagner

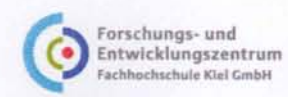


Smart Materials and Structures

2nd International Workshop Kiel, 29. – 31. August 2007









INTERREG III A



FYNSAMT • K.E.R.N.

2nd international Workshop on Smart Materials and Structures, Kiel-Germany August 29-31, 2007

			Room: 7			
8:30 K	Setter: Small ferroelectric structures					
9:10 l	Šittner: Functional properties of	of ultrathin Ni	Ti shape memory alloy wires			
Break: Coff	ee / Tea					
10:00 - 11:50	Dielectrics	10:00 - 12:10	Nanostructured materials III			
	Chair: N. Mathur Room: 7		Chair: Rubahn Room: 8			
10:00 I	Wang: Low loss dielectric composites for RF and microwave applications	10:00 I	Rubahn: Organic nanosensors: Development and implementation			
10:30 T	Banys: Dielectric dispersion in nanograin PMN ceramics: comparison with PMN nanopowders	10:30 T	Wu: Preparation and characterization of Co-BaTiO₃/MgO(100) and Co-BaTiO₃/Si(100) nano-composite films			
10:50 T	Lente: Intrinsic and extrinsic contributions to the dielectric response in ordinary and relaxor ferroelectric ceramics	10:50 T	Strunskus: Polymer-metal nanocomposites for functional applications			
11:10 T	Thongbai: Giant dielectric response in CaCu ₃ Ti ₄ O ₁₂ /(Li, Ti)-doped NiO nanocomposites subjected to post-sintering and uniaxial stress	11:10 T	Larsen: Nano structured polymers with proton conductivity			
11:30 T	Jha: Impedance-spectroscopy analysis of Ba ₅ SmTi ₃ Nb ₇ O ₃₀ ferroelectric ceramics: Effect of sintering conditions	11:30 T	Lanceros-Méndez: Electroactive polymer micro- and nano-composites based on PVDF			
		11:50 T	Maensiri: Fabrication, characterization and magnetic properties of electrospun Fe-doped TiO ₂ nanofibers			

Thursday, 2007-08-30	11.10	Talk	Dielectrics	Room: 7
----------------------	-------	------	-------------	---------

Giant dielectric response in CaCu₃Ti₄O₁₂/(Li, Ti)-doped NiO nanocomposites subjected to post-sintering and uniaxial stress

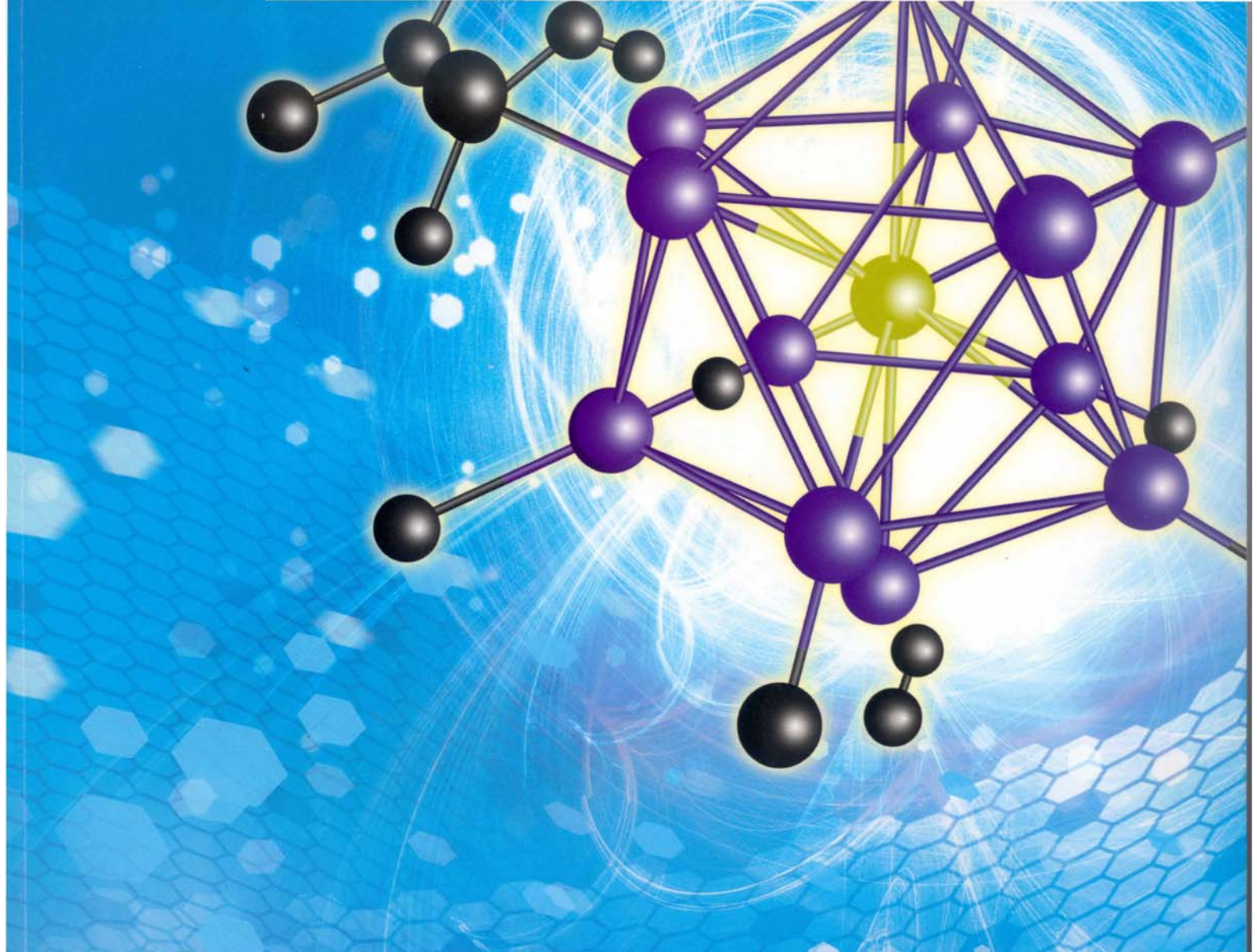
Prasit Thongbai¹, S. Maensiri¹, Teerapon Yamwong², and Rattikorn Yimnirun³

This paper reports the influences of the post-sintering annealing in argon and uniaxial compressive pre-stress on the giant dielectric properties of the CaCu₃Ti₄O₁₂-Li_{0.3}Ti_{0.02}Ni_{0.68}O nanocomposites ceramics sintered at 1100 °C in air for 16 h. The giant values of the dielectric permittivity as high as $\varepsilon \sim 10^5$ at various frequencies (f =100 kHz-1 MHz) over a broad temperature range of -50 to 190 ℃ have been observed in polycrystalline CaCu₃Ti₄O₁₂ ceramics that are reinforced with small amount of Li_{0.3}Ti_{0.02}Ni_{0.68}O nanoparticles of 39 nm. The dielectric behavior of CaCu₃Ti₄O₁₂ and CaCu₃Ti₄O₁₂-Li_{0.3}Ti_{0.02}Ni_{0.68}O nanocomposites exhibits Debye-like relaxation which can be interpreted based on Maxwell-Wagner model and discussed based on internal boundary layer capacitor effect. Postsintering annealing in argon for 5 h lead to a significant increase in €' for CaCu₃Ti₄O₁₂ ceramic but a slight decrease in & for the CaCu3Ti4O12-Li03Ti002Ni0.68O nanocomposite ceramics. The dielectric properties of the argon-annealed samples change significantly with the applied compressive stress (the absolute change can reach 16% at a maximum stress of 130 MPa). However, the changes in dielectric properties with the stress in the samples subjected to different amount of Li_{0.3}Ti_{0.02}Ni_{0.68}O follow opposing trends. The mechanisms responsible for this difference are discussed.

¹ Integrated Nanotechnology Research Center (INRC), Khon Kaen University and Small & Strong Materials Group (SSMG), Department of Physics, Faculty of Science, Khon Kaen University, Khon Kaen, Thailand

² National Metals and Materials Technology Center (MTEC), Thailand Science Park, Pathumthani, Thailand

³ Department of Physics, Faculty of Science, Chiang Mai University, Chiang Mai, Thailand



IEEE International NanoElectronics Conference

3–8 January 2010 City University of Hong Kong

Synthesis of Nanocrystalline Li_{0.05}In_{0.05}Ni_{0.90}O Powder and Its Bulk Giant Dielectric Properties

Prasit Thongbai^{1,*}, Tanachat Eknapakul¹, Sarawut Pongha¹, Teerapon Yamwong², and Santi Maensiri¹

Abstract- Li $_{0.05}$ In $_{0.05}$ Ni $_{0.90}$ O (LINO) nanoparticles of 100-300 nm were successfully prepared by a direct thermal decomposition method. X-ray diffraction and scanning electron microscopy were used to characterize the phase formation and microstructure of the LINO powder and ceramic, respectively. Dense LINO ceramic was obtained by sintering the LINO nanocrystalline powder at 1200 °C for 4 h . Giant dielectric properties of the sintered LINO ceramic were investigated as functions of temperature and frequency and can be ascribed to the interfacial polarization mechanism and the small polaron hopping inside the grains.

I. INTRODUCTION

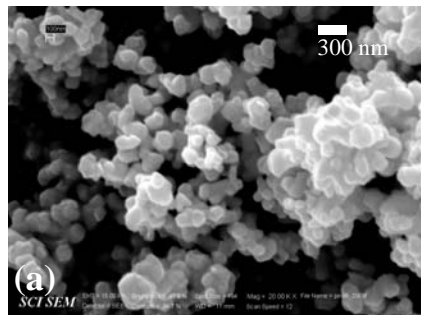
High-permittivity dielectric materials with good thermal stability and Ba/Pb-free have been playing a significant role in microelectronics, since they have been used as important elements in capacitors and memory devices. In recent years there have been many intensive researches to investigate new high dielectric materials because they might offer the opportunity to increase the choices of materials for various practical applications. High permittivity NiO-based ceramics, a non-perovskite, and non-ferroelectric materials, $A_x B_y Ni_{1-x-y} O$ (where A are monovalents of Li, Na, K and B are Ti, Al, Ta, Si) [1-7], have attracted considerable attentions in recent years due to their impressive high apparent dielectric permittivity (ε') of 10³-10⁵, which remains constant in the temperature range of -50 to 150 °C [1,5]. Moreover, the dielectric properties of such material systems can be tuned by changing the composition of the additive of A and B [1]. However, an explanation of such high dielectric permittivity is still unclear and uncompleted. Therefore, it is vary important to search the new giant dielectric materials of NiO-based ceramic systems and attempt to clarify the origin of the giant ε' and the polarization relaxation behavior of these ceramic.

In this present, we prepared the LINO nanocrystalline powder by a direct thermal decomposition method. Dense LINO ceramic can be obtained by sintering the LINO nanopowder. It was revealed that the LINO ceramic exhibited the giant dielectric properties, which were attributed to the internal barrier layer effect (IBLC) combined with the hopping of charge carrier in the grain interiors.

II. EXPERIMENTAL

(CH₃COO)₂Ni.4H₂O, C₂H₃LiO₂.2H₂O, and InC₆H₉O₆, were employed as starting raw materials. The nanocrystalline LINO powder was simply prepared by the following procedure. Firstly, stoichiometric amounts of the starting powders were dissolved in distilled water and mixed in alumina crucible. Then, the mixed powder was decomposed at a temperature of 650 °C for 10 h. The LINO powder was pressed into pellet of 9.5 mm in diameter and ~1-2 mm in thickness. Finally, this pellet was sintered at 1200 °C for 4 h.

The sintered ceramic was characterized by X-ray diffraction (XRD) and scanning electron microscopy (SEM). The LINO ceramic was polished and electroded by silver paint. It was allowed to dry overnight. The dielectric response of the sample was measured using a Hewlett Packard 4194A impedance gain phase analyzer over the frequency ranging from 100 Hz to 10 MHz and at the oscillation voltage of 1.0 V. The measurement was performed over the temperature ranging from -60 to 50 $^{\circ}\mathrm{C}$ using an inbuilt cooling–heating system. Each measured temperature was kept constant with an accuracy of ± 1 $^{\circ}\mathrm{C}$.



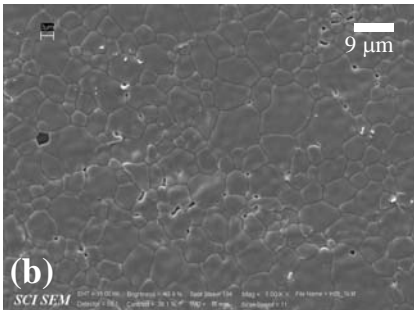


Fig. 1. SEM images of Li_{0.05}In_{0.05}Ni_{0.90}O (a) powder and (b) ceramic.

¹Small & Strong Materials Group (SSMG), Department of Physics, Faculty of Science, Khon Kaen University, Khon Kaen, 40002, Thailand

²National Metals and Materials Technology Center (MTEC), Thailand Science Park, Pathumthani, 12120, Thailand

^{*}Contacting Author: Mr. Prasit Thongbai; Email address: prasitphysics@hotmail.com; Tel.: +66-43-202222 to 9 ext. 2248; Fax: +66-43-202374

III. RESULTS AND DISCUSSION

Morphology of the calcined LINO powder and ceramic is revealed by SEM as shown in Fig. 1. The powder, shown in Fig. 1(a), is in a nearly spherical shape and of sizes of about 100–300 nm. Some agglomerates are observed in the calcined powder. Sintering of LINO nanopoder results in a bulk LINO ceramic with good microstructure. The SEM micrograph of the LINO ceramic, shown in Fig. 1(b), reveals that the LINO ceramic is dense and has obvious grain and grain boundary structure.

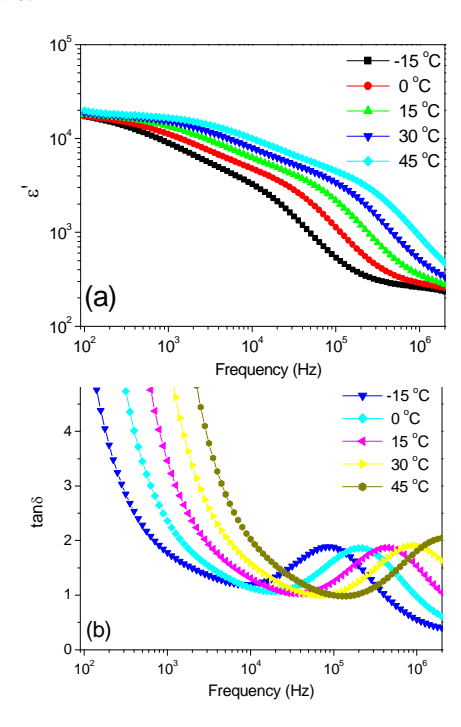


Fig. 2. Frequency dependence of (a) dielectric constant ϵ' and (b) loss tangent $\tan\delta$ at different temperatures for the LINO ceramic.

As demonstrated in Figs. 2(a) and 2(b), the ε' shows the high values at low frequencies, and it rapidly decreases if the frequency is sufficiently high. Two sets of thermally activated relaxations are observed, i.e., low- (LFDR) and high- (HFDR) frequency dielectric relaxations. These two step decreases shift to higher frequency with increasing the temperature, corresponding to the movement of the tanδ peaks. The LFDR is identified to originate from the internal barrier-layer capacitor effects related to the grain boundaries [8], and the HFDR is ascribed to the dipolar effects induced by charge-carrier-hopping motions inside the grains [9].

IV. CONCLUSION

In conclusion, the LINO nanocrystalline powder was successfully prepared by a direct thermal decomposition method. Dense LINO ceramic can be obtained by sintering the LINO nanopowder. Our result revealed that the LINO ceramic exhibited the giant dielectric constant, which was attributed to

the internal barrier layer capacitance (IBLC) effect combined with the hopping of charge carrier in the grain interiors.

ACKNOWLEDGMENT

P. Thongbai would like to thank The National Science and Technology Development Agency for financial supports of his studies through the TGIST Programs, respectively. This work was financially supported by the Thailand Research Fund and the Commission on Higher Education, Thailand.

REFERENCES

- J. Wu, C. W. Nan, Y.-H Lin and Y. Deng, "Giant Dielectric Permittivity Observed in Li and Ti Doped NiO," *Phys. Rev. Lett*, vol. 89, p.217601, 2002.
- [2] S. Maensiri, P. Thongbai and T. Yamwong, "Giant dielectric response in (Li, Ti)-doped NiO ceramics synthesized by the polymerized complex method," *Acta. Mater*, vol. 55, pp. 2851-2861, 2007.
- Y.-H. Lin, J. Wang, L. Jiang, Y. Chen and C. W. Nan, "High permittivity Li and Al doped NiO ceramics," *Appl. Phys. Lett*, vol. 85, p. 5664, 2004.
 Y.-H. Lin, L. Jiang, R. Zhao and C. W. Nan, "High-permittivity core/shell
- [4] Y.-H. Lin, L. Jiang, R. Zhao and C. W. Nan, "High-permittivity core/shell stuctured NiO-based ceramics and their dielectric response mechanism," *Phys. Rev. B*, vol. 72, p. 014103, 2005.
- [5] P. K. Jana, S. Sarkar and B. K. Chaudhuri, "Low loss giant dielectric and electrical transport behavior of K_xTi_yNi_{1-x-y}O system," *Appl. Phys. Lett*, vol. 88, p. 182901, 2006.
- [6] P. K. Jana, S. Sarkar, H. Sakata, T. Watanabe and B. K. Chaudhuri, "Microstructure and dielectric properties of Na_xTi_xNi_{1-x-y}O (x = 0.05–0.30, y = 0.02)," *J. Phys D: Appl Phys*, vol. 41, p. 065403, 2008.
- [7] Y. J. Hsiao, Y. S. Change, T. H. Fang, T. L. Chai, C. Y. Chung, et al, "High dielectric permittivity of Li and Ta codoped NiO ceramics," J. Phys D: Appl Phys, vol. 40, pp. 863-868, 2007.
- [8] C. C. Wang, Y. M. Cui and L. W. Zhang, "Dielectric properties of TbMnO₃ ceramics," Appl. Phys. Lett, vol. 90, p. 012904, 2007.
- [9] P. Wu, V. Ligatchev, Z. G. Yu, J. Zheng, M. B. Sullivan, et al, "Defects in codoped NiO with gigantic dielectric response," *Phys. Rev. B*, vol. 79, p. 235122, 2009.

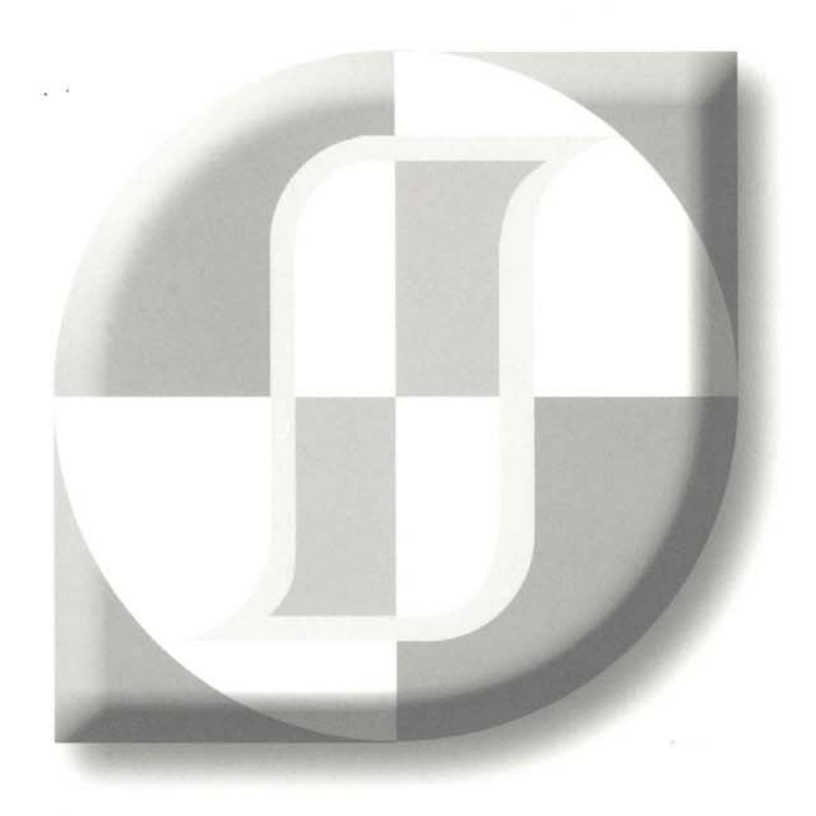
$Contributed\ Presentations-Thursday-Jan\ 7,\ 2010-IEEE\ INEC\ 2010$

23-65104741; email: hucg@cqu.edu.cn)	
Synthesis of Hierarchically Organized Nanostructured TiO ₂ by Pulsed Laser Deposition and	
Its Application to Dye-sensitized Solar Cells	
Jun Hong Noh ¹ , Jong Hun Park ¹ , Hyun Soo Han ¹ , Sangwook Lee ¹ , Dong Hoe Kim ¹ , Hyun Suk Jung ² , Kung Sun Hong ¹	FP438
Department of Materials Science & Engineering, Seoul National University, Seoul 151-742, Korea	
² School of Advanced Materials Engineering, Kookmin University, Jeongneung-dong, Seongbuk-gu,	
Seoul 136-702, S. Korea	
Synthesis of Nanocrystalline Li _{0.05} In _{0.05} Ni _{0.90} O Powder and Its Bulk Giant Dielectric	
Properties	8
Prasit Thongbai ¹ ,*, Tanachat Eknapakul ¹ , Sarawut Pongha ¹ , Teerapon Yamwong ² , and Santi Maensiri ¹	
¹ Small & Strong Materials Group (SSMG), Department of Physics, Faculty of Science, Khon Kaen	FP439
University, Khon Kaen, 40002, Thailand 2National Metals and Materials Technology Center	
(MTEC), Thailand Science Park, Pathumthani, 12120, Thailand* Contacting Author: Mr. Prasit	
Thongbai; Email address: prasitphysics@hotmail.com; Tel.: +66-43-202222 to 9 ext. 2248; Fax:	
+66-43- 202374	
Synthesis of Ni/TiO2 Nanocomposite by Loading TiO2 Nanotubes with Ni Nanoparticles	
Yannan Yanga, Yunhuai Zhanga, Peng Xiaob*, Xiaoning Zhanga, Lu Lua and Lu Lia	
^a Department of Chemical Engineering, Chongqing University, Chongqing, 400030, P.R. China	FP440
^b Department of Physics, Chongqing University, Chongqing, 400030, P.R. China *Contacting	FP440
Author: Peng Xiao is with Department of Physics, Chongqing University, P.R. China (phone:	
+86-15823038874; fax: +86-023-6510- 2031; email: yangyannanyin@yahoo.com.cn).	
Synthesis of Oxidized Graphene Sheets with High Surface Area by Modified Thermal	
Exfoliation Method under Ultra-low Temperature	
Haobin Zhang, Yong Yang, Jiwen Wang, Zhaohui Lu, Cao Chen, Wenge Zheng*, Qing Yan and	
Shuai Yin	FP441
Ningbo Key Laboratory of Polymer Materials, Polymers and Composites Division Ningbo Institute	
of Material Technology & Engineering, Chinese Academy of Sciences, Ningbo 315201, P.R.China	
E-mail address: polang@nimte.ac.cn or wgzheng@nimte.ac.cn (Wenge Zheng)	
Synthesis of Si Nanowries and their Hysteresis Behavior	
Tae-Eon Park, 1,2 Myoungha Kim, 1 Hwangyou Oh, 1 Il-Soo Kim, 1 Joonyeon Chang, 2 Suk-Hee Han, 2	
and Heon-Jin Choi ¹ *	
¹ Department of Materials Science and Engineering, Yonsei University, Seoul, Korea ² Center for	FP442
Spintronics Research, Korea Institute of Science and Technology, Seoul, Korea *Contacting Author:	
Heon-Jin Choi is with the Department of Materials Science and Engineering, Yonsei University,	
Seoul, Korea (phone: +82-2-2123-5849; email: hjc@yonsei.ac.kr)	
The Analysis of X-Ray Diffraction by Al3+ Implanted Polytetrafluorethylene	
Yuan Zhao, Hui Tang, and Feng C. Wang	
School of Material Science and Engineering, Harbin University of Science and Technology, Harbin,	FP443
China. *Contacting Author: Hui Tang is with the School of Material Science and Engineering,	wardentellen.
Harbin University of Science and Technology, Harbin, China. (phone: +86-13936418364; email:	
zhaoyuan1986@tom.com)	
The Effect of X-ray Irradiation on the Novella Type Photoresist	FP444
Hsin-Chiang You ¹ *, Shao-Hui Shieh ¹ , Shiang-Jun Zhang ¹ , Fu-Hsiang Ko ² , Hsiung-Min Lin ² ,	

AMC2008

Asian Magnetics Conference 2008

December 10-13, 2008, Paradise Hotel, Busan, Korea



Hosted by

The Korean Magnetics Society

Sponsored by

Korea Research Foundation Korea Science and Engineering Foundation Korean Federation of Science and Technology Societies

The Korean Magnetics Society

AP10

(1-x)CaCu₃Ti₄O₁₂-xSr_{0.7}La_{0.3}Fe_{11.7}Co_{0.3}O₁₉ Composites Magnetic and Giant Dielectric Properties of

Integrated Nanotechnology Research Center (INRC), and Small & Strong Materials Group (SSMG), Prasit Thongbai1*, Teerapon Yamwong2, and Santi Maensin1

National Metals and Materials Technology Center (MTEC). Thailand Science Park. Pathumthani, 12120. Thailnad Department of Physics, Khon Kaen University, Khon Kaen, 40002, Thailand

*Corresponding author: e-mail: prasitphysics@hotmail.com

In this study, the (1-x)CaCu,Ti₄O_{12-x}Sr₀7La_{0.3}Fe_{11.7}Ca_{0.3}O₁₉ (when x = 0, 0.1, 0.3, 0.5, 0.7, 0.9, and 1) ceramic composites are prepared by a conventional mixed-oxide method. The microstructure and phase composition of the ceramic composites are characterized by x-ray diffraction (XRD) and scanning electron microscopy (SEM), respectively. The dielectric properties of the ceramics are measured as functions of both temperature (-50 - 200 "C) and frequency (102 - 10" Hz). All of the samples exhibit a high low-frequency dielectric permittivity, which is mainly attributed to the Maxwell-Wagner polarization sample magnetometry (VSM) at room temperature. Our results reveal that the magnetization increases with the mechanism and thermally activated mechanism. The magnetic properties of the ceramics are determined using vibrating StarLausFerraConsOry phase increasing.

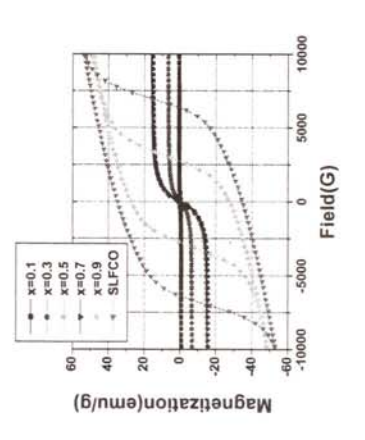


Fig. 1 Magnetization of the sintered (1-x) CCTO- x SLFCO composites as a function of field, measured at room

AP11

Magnetic Properties of NiO Thin Films Synthesized by Reactive Sputtering

Hyemin Shin, Yun man Lee, Sanghwa Lee, and Jae-yong Kim*

Department of Physics, Hanyang University, Seoul, Korea

*Corresponding author: e-mail: Kimjy(a)hanyang.ac.kr

antiferromagnetic film has advantages over other antiferromagnetic films due to its high blocking temperature. Although NiO Nickel Oxide (NiO) is considered to be a promising candidate for semiconductor with p-type conductivity (3.6 ~ 4.0 eV band-gap). Also, NiO is an interesting material to study magnetic properties, because it has been known for some time that small particles (less than 100 nm) of NiO show superparamagnetism that increases as the particle size decreases and NiO thin films have a wide range of applications because of excellent optical, electrical properties with chemical stability, many researches on NiO contain mainly related with its crystalline structure, preferred orientation and lack of magnetic behavior.

We have prepared NiO thin films on Si (100) substrate using a Ni target at various O2 / Ar ratios, substrate temperatures and applied powers. The NiO thin film was synthesized by RF and DC reactive magnetron sputtering methods. The effect of process parameters were investigated in terms of crystallographic structures. The X-ray diffraction pattern shows that the sample synthesized at the substrate temperature of 573 K in the partial pressure of 25 % for oxygen content and applied power of 270 W forms a single NiO phase. The magnetic properties of samples were investigated by measuring magnetization as a function of magnetic field by using a vibrating sample magnetometer, and the results will be presented.



AD04	15:30	Novel Multibit Magnetic Tagging Techniques for High-Throughput Multiplexed Chemical Analysis
AD05	15:45	Effects of Metal Ions on the Intrinsic DNA Magnetisms
AD06	16:00	Magnetic Nanoparticles for Biomolecular Detection, Manipulation, and Imaging

• Dec. 10, 2008 (Wednesday) 13:30~17:30 Magnetic Oxides and Applications

Capri Room

Chair: JongHoon Jung

		Chair : jongroon jun	0
AP01	Poster	Fabrication of Carbonyl Iron Embedded Polycarbonate Composite Particles and Magnetorheological Characterization Fei Fei Fang, Ying Dan Liu, and Hyoung Jin Choi*	18
AP02	Poster	Fabrication and Mössbauer Characterization of MgFe $_2$ O $_4$ /Fe $_3$ O $_4$ Composite Nano-particles $^{\cdot\cdot}$ LI Zhi-Wei, WANG Hai-Bo, SUN Jian-Rong, GAO Yuan, and LI Fa-Shen*	19
AP03	Poster	Withdrawn	
AP04	Poster	Withdrawn	
AP05	Poster	Fabrication and Magnetic Properties of Fe65Co35-B2O3 Granular Films for High Frequency Application Yuhua Xiao, Shihui Ge*, Bangming Zhang, Guowei Wang, and Huaping Zuo	20
AP06	Poster	Cogging Force Reduction of a Stationary Discontinuous Armature PM-LSM by Magnet Segmentation Yong-Jae Kim*, Youn-Ok Choi, and Geum-Bae Cho	21
AP07	Poster	Influence of flux Barrier arc and slot to pole combination for wide speed range on the Interior Permanent Magnet Synchronous Motor Jae-Hak Choi*, Yon-Do Chun, Pil-Wan Han, Dae-Hyun Koo, and Jang-Sung Chun	21
AP08	Poster	Technological Role of Indium in Nickel-zinc Nano Ferrites Synthesized Via Oil-in-water Micelle Technique Sangeeta Thakur*, S.C.Katyal, Patrick Quéffélec, Jean Löaec, and M. Singh	22
AP09	Poster	Enhanced Performance of MFL Tool by Adopting New Design of Magnetizing System	22
AP10	Poster	Magnetic and Giant Dielectric Properties of (7-x)CaCu ₃ Ti ₄ O ₁₂ -xSr _{0.7} La _{0.3} Fe _{11.7} Co _{0.3} O ₁₉ Composites Prasit Thongbai*, Teerapon Yamwong, and Santi Maensiri	23
AP11	Poster	Magnetic Properties of NiO Thin Films Synthesized by Reactive Sputtering	23
AP12	Poster	Crystallographic and Magnetic Properties of $\alpha\text{-LiFeO}_2$ Seung Wha Lee and Chul Sung Kim*	24
AP13	Poster	Magnetization Processes of (La _{0.7} Pb _{0.3} MnO ₃) _{1-x} (SiO ₂) _x Composites ······ S. L. Young*, C. H. Lin, H. Z. Chen, C.R. Ou, M. C. Kao, and Lance Horng	24
AP14	Poster	New Synthetic Route of Single-phase Z-type (Ba ₃ Co ₂ Fe ₂₄ O ₄₁) Hexaferrite Particles S. Bae, Y. K. Hong*, J. J. Lee, J. Jalli, G. S. Abo, A. Lyle, I. T. Nam, W. M. Seong, and G. H. Kim	25

NANOSMAT2009 NANOSMAT2009 NANOSMAT2009 NANOSMAT2009

NANCSMAT2000 MANOSMAT2009

NAN

NAN

NAN

NAN

NAN

4th International Conference on Surfaces, Coatings and Nanostructured Materials (NANOSMAT 2009)

ABSTRACTS BOOK

Editors:

Dr N. Ali (UK) & Dr R. Polini (Italy)

NANOSMAT2009 NANOSMAT2009

Advanced Nano-Materials Research Team, Division of Nano & Bio Technology, Daegu Gyeongbuk Institute of Science and Technology, 5th Floor, Daegu Technopark Venture 2 Plant, 75 Gongdanbuk 2gil, Dalseo-gu, 704-230, Daegu, Republic of Korea

Interest in nanostructure made from semiconducting oxide materials are exponentially grown on the last years, due to their attracting potential application in electronic, optical and sensor field. Additionally, to apply semiconducting oxide materials on various electronic devices, it is important to understand its electrical properties and interaction with semiconductor-metal contacts. Cause we have focused our attention on the electrical properties of individual zinc oxide nanorod (NR). Single crystal nanostructures were synthesised with the aim of exploring and studying their capabilities as nano-sized sensors on form of individual NR sensors. The ZnO NRs for this work were synthesized by micro emulsion methods. The solution of isopropyl alcohol suspended with the ZnO NR was dispersed on a pre-patterned p-type silicon wafer with a 100 nm silicon oxide layer. After that electrodes of Ti/Au, which connect the NR to the electrodes, were patterned by using electron beam lithography and conventional lift-off method. Then we using bi-layer electron beam resist structure, copolymer / poly-methyl-methacrylate (PMMA), was used to make the good under-cut for the metal lift-off process. The electrical properties were measured using a source measure unit (4200SCS, Keithley) equipped with shielded probe station. ZnO NR device shows nonlinear and asymmetrical behaviour. These data proved to different measurements of the same device at different time gaps after fabrication, which shows that the rectifying property of the device is stable. According to the rectifying current voltage curves, the device can be considered as an effective diode, a turn-on voltage of 4V for the forward bias was found. We will present and overview of the device characteristic data that have been made and detailed possible rectifying mechanism of ZnO single NR device.

M. H. Huang, et al., Science, 292, 1897 (2001).

NS397: Effect of Nanocrystalline Film Existing on Surface of (Li, Ti)-doped NiO Ceramics on Their Dielectric Properties

P. Thongbai¹, T. Yamwong², S. Maensiri¹

Effect of nanocrystalline film with grain size of $^{\sim}100-200$ nm existing on the surface of $L_{i_x}T_{i_y}N_{i_1.x.y}O$ (LTNO) ceramics on their giant dielectric properties was investigated as functions of frequency and temperature. X-ray diffraction and scanning electron microscopy with energy dispersive x-ray spectrometer were used to characterize the phase formation, microstructure, and chemical compositions of the grain interior, grain boundary, and surface layer of the LTNO ceramics, respectively. The microstructure analysis revealed that Ti doping was rich at the grain boundary region and the outmost surface layer, forming the nanocrystalline film. It was found that such nanocrystalline film had a remarkable influence on the dielectric properties of the LTNO ceramics. Two thermally activated dielectric relaxations were detected in the dielectric spectra of the LTNO ceramics, i.e., the high— and low—frequency relaxations (abbreviated as HFR and LFR, respectively). Interestingly, when the nanocrystalline films were removed from the both sides of the LTNO samples, the LFR disappeared, whereas the electrical properties of the remaining HFR did not change. The LFR was identified to originate from the interfacial polarization related to the insulating nanocrystalline film. The HFR might be attributed to the internal barrier—layer capacitor effect associated with the grain boundaries [1, 2] or/and the small polaron hopping inside the grains [3].

¹Department of Physics, Faculty of Science, Khon Kaen University, Khon Kaen, 40002, Thailand.

²National Metals and Materials Technology Center (MTEC), Thailand Science Park, Pathumthani, 12120, Thailand.

- [1] J. Wu, C.W. Nan, Y. Lin and Y. Deng, Phys. Rev. Lett., 89, 217601 (2002).
- [2] P. Thongbai, S. Pongha, T Yamwong and S. Maensiri, Appl. Phys. Lett., 94, 022908 (2009).
- [3] Wu, V. Ligatchev, Z.G. Yu, J. Zheng, M.B. Sullival and Y. Zeng, Phys. Rev. B, 79, 235122 (2009).

NS398: Fabrication and Characterization of Carbon Nanotubes (CNTs) Reinforced Nylon 6 Composite Filaments

P. Saengkwamsawang, S. Pimanpaeng, V. Amornkitbamrung, S. Maensiri

Integrated Nanotechnology Research Center (INRC), and Department of Physics, Faculty of Science,

Khon Kaen University, Khon Kaen, 40002, Thailand

We report a method to fabricate COOH-functionalized carbon nanotubes (CNTs) and pristine CNTs reinforced Nylon 6 composite filaments through an extrusion process. Neat Nylon 6 and Nylon 6 reinforced with 0.5-1 wt% CNTs are dry mixed and extruded by a single screw extrusion method. X-ray diffraction (XRD) results indicate that neat Nylon 6 filament exhibits y- phase while all the CNTs reinforced Nylon 6 composite filaments show α-phase. Thermo gravimetric analysis (TGA) shows the decomposition temperature of CNTs reinforced Nylon 6 composite filaments increases with increasing of infusing rate. It is observed that the CNTs reinforced Nylon 6 filaments are more thermally stable than the neat Nylon 6 filament. Fourier transform infrared spectroscopy (FTIR) reveals that CNTs enhance the bond strength to Nylon 6 polymer chain with C-N amines, C-H amines, C-H Alkanes and also O-H of compound type for COOH functionalized CNTs. Tensile tests on single filaments have demonstrated that tensile strength at break of CNTs reinforced Nylon 6 composite filaments compared to that of the neat Nylon 6 increases about 13-52%, whereas the percent elongation at break decreases about 48-54 % with increasing infusing rate. Scanning electron microscopy (SEM) reveals the tensile fractured surface of CNTs reinforced Nylon 6 composite filaments showing brittle behavior with crazing. It is found from this work that the CNTs can affect the tensile behavior of Nylon 6, and the bonds interfacial between CNTs and Nylon 6 matrix plays an important role in mechanical properties of CNTs reinforced Nylon 6 composite filaments.

NS399: Synthesis and Structure Analysis of La_{0.5}Sr_{0.5}TiO₃ Nanoparticles Prepared by Thermal Decomposition Method

E. Swatsitang^{1,2}, P. Buppato¹, S. Maensiri^{1,2}

 $La_{0.5}Sr_{0.5}TiO_3$ (LSTO) nanoparticles were synthesized by thermal decomposition method using Cl_3La , $Cl_2Sr \cdot 6H_2O$ and $C_{16}H_{28}O_6Ti$ as starting materials. The obtained precursors in powder form were sintered at 700, 900, 1100 and 1300 °C for 3, 6 and 9 hours in air. The structures of all samples were analyzed by XRD

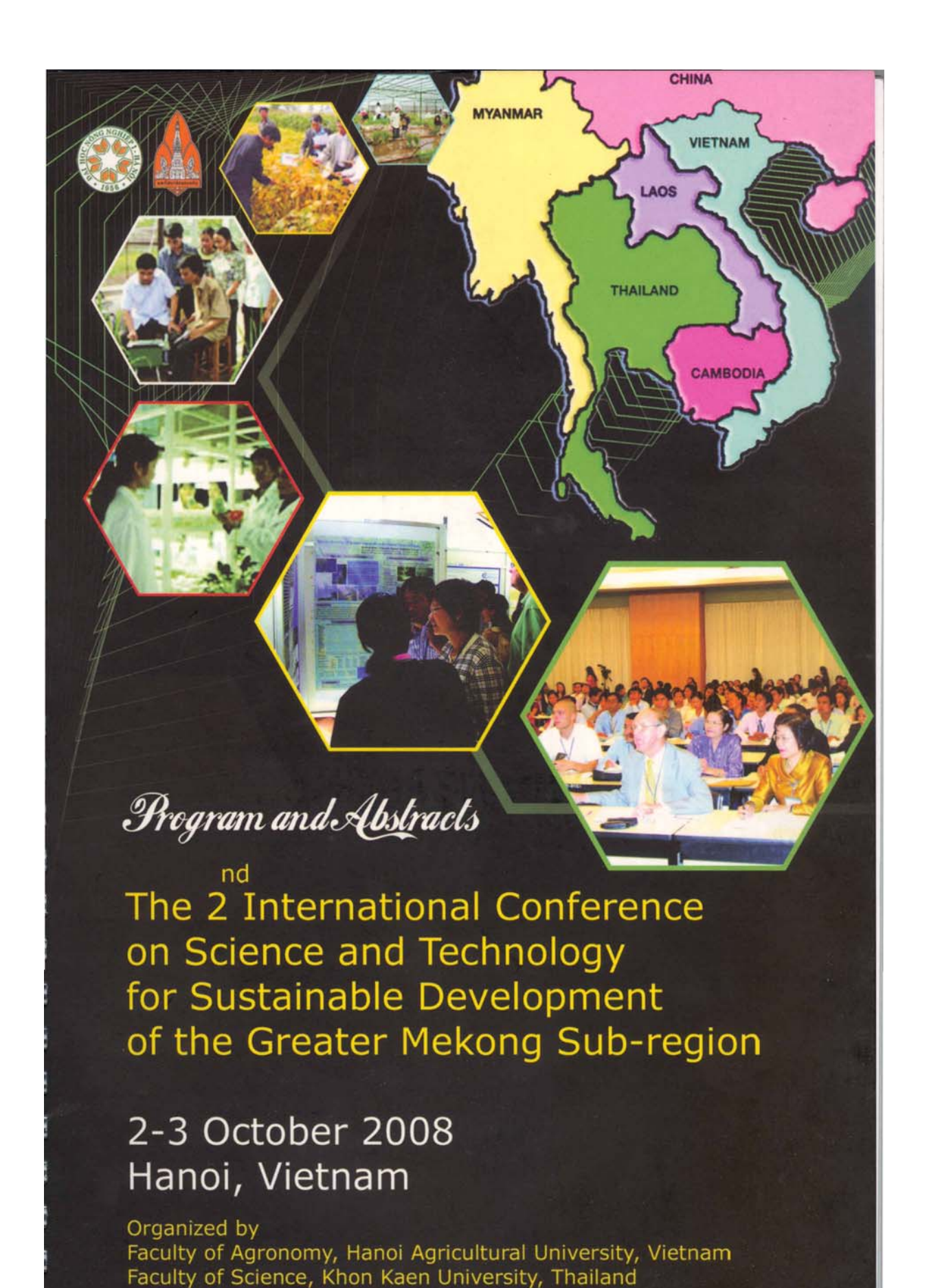
Department of Physics, Faculty of Science, Khon Kaen University, Khon Kaen, 40002, Thailand

Integrated Nanotechnology Research Center (INRC), Faculty of Science, Khon Kaen University, Khon Kaen, 40002, Thailand

15:45 - 16:00	NS135: Manuela Mura, King's College, London, UK "The role of dispersion interactions on self assembly of flat molecules on metallic substrate"
16:00 - 16:15	NS263: Jessica Rodríguez Fernández, Ludwig-Maximilians-Universität München, Germany "Embedding gold nanorods in thermoresponsive microgels for optothermally-driven applications"
16:15 - 16:30	NS320: C.E. Pastore, Universidad de Cádiz, Spain "Influence of In content on defects and spinodal decomposition in InxGa1-xP layers grown on Ge substrates"
16:30 - 16:45	NS338: Piotr Jedrasik, Chalmers University of Technology, Sweden "Nanoengineering of highly ordered three-dimensional polyaniline nanoarchitectures"
16:45 - 17:00	NS350: Jin Soo Kim, Chonbuk National University, Korea "Carrier Repopulation Process for the Seven-stacked InAs/InAlGaAs Quantum Dots"
17:00 - 17:15	NS397: Prasit Thongbai, Khon Kaen University, Thailand "Effect of Nanocrystalline Film Existing on Surface of (Li, Ti)-doped NiO Ceramics on Their Dielectric Properties"
17:15 – 17:30	NS154: Markus Bruehl, RWTH Aachen University, Germany "Electromagnetic Properties of Novel Thermal Sprayed NiZn-Ferrite Coatings for Electromagnetic Applications"
17:30 - 19:30	Poster Session II
20:00	Conference banquet

22 October 2009

Time	INVITED SESSION
08:30 - 09:00	Chairperson(s): Professor J. De-Hosson (Netherlands) & Dr R. Polini (Italy) Room(s): FORO TRAIANO+ADRIANO 1) Dr Sastry Cheruvu, Southwest Research Institute, San Antonio, USA "Nanocrystalline coatings for ultra supercritical boiler and turbine components"
09:00 - 09:30	2) Dr Ronghua Wei, Southwest Research Institute, USA "Long Term Effect of Nitride Barrier Layers on Inward Al Diffusion of MCrAl Nanocoatings at Temperatures up to 1010 °C"
09:30 - 10:00	3) Dr Moritz Graf zu Eulenburg, Coatema Coating Machinery GmbH, Germany "Nanocoating close to the market"
10:00 - 10:30	4) Professor K. Pourrezaei, Drexel University, USA "Rapid Application & Commercialisation of nanotechnology to stimulate economic growth"
10:30 - 11:00	Refreshments



EFFECT OF TI DOPING ON THE ELECTRICAL AND HIGH DIELECTRIC PROPERTIES OF (Li, Ti)-doped NiO CERAMICS PREPARED BY A SIMPLE PVA SOL-GEL METHOD

Prasit Thongbai1*, Teerapon Yamwong2 and Santi Maensiri1

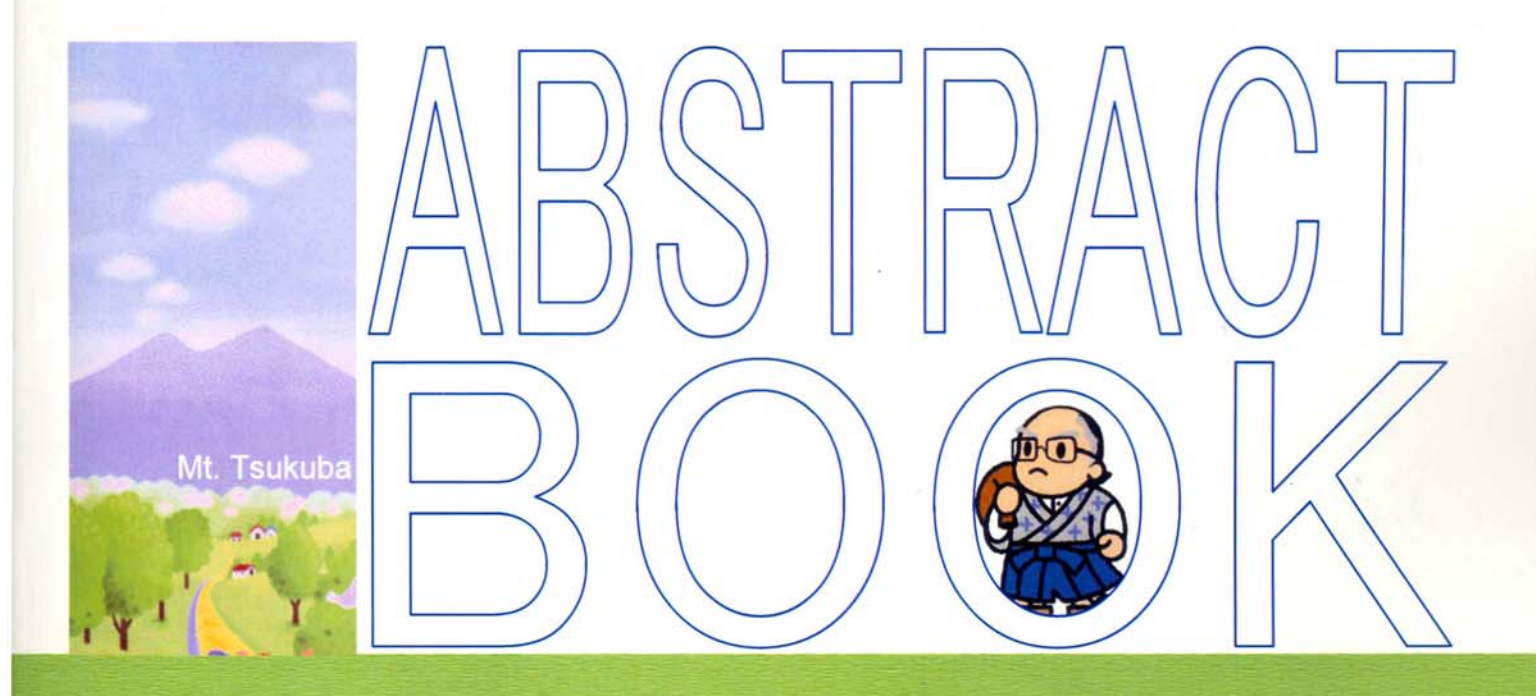
¹ Integrated Nanotechnology Research Center (INRC), and Small & Strong Materials Group (SSMG), Department of Physics, Khon Kaen University, Khon Kaen 40002, Thailand.
² National Metals and Materials Technology Center (MTEC),
Thailand Science Park, Pathumthani 12120, Thailand.

E-mail: prasitphysics@hotmail.com

Giant dielectric-permittivity $\text{Li}_{0.05}\text{Ti}_x\text{Ni}_{0.95\text{-x}}\text{O}$ (when x = 0.05 and 0.10) ceramics were prepared by a simple PVA sol-gel method. The dielectric properties were investigated as a function of frequency (10^2-10^6 Hz) at various temperatures (-60-150 °C). Both ceramic samples exhibit a high low-frequency dielectric permittivity ($\varepsilon_0'\sim0.47\text{-}1.2\times10^4$). Our results reveal that the concentration of Ti has a remarkable effect on the dielectric properties of the $\text{Li}_{0.05}\text{Ti}_x\text{Ni}_{0.95\text{-x}}\text{O}$ ceramics. A frequency dielectric dispersion phenomenon in $\text{Li}_{0.05}\text{Ti}_x\text{Ni}_{0.95\text{-x}}\text{O}$ ceramics was also analyzed by impedance spectroscopy. A separation of the grain and grain boundary properties was achieved using an equivalent circuit model. Interestingly, the activation energy required for relaxation is almost the same as the grain conduction activation energy. Through the analysis by impedance spectroscopy, it is strongly believed that the high dielectric permittivity response of the LTNO is attributable to the Maxwell-Wagner polarization mechanism.

PACS numbers(s): 77.22.Ch, 77.22.Gm, 77.84.Dy

Poster Presentations		
P-01	Simple proofs of determining all nonisomorphic Monoids of order 3	77
	Somehit Chotchaisthit	
P-02	Skew idempotents in order-preserving transformation semigroups	78
	Tawhat Changphas and Boonyen Thongkam	
P-03	Rate of composting and quality of compost under different	79
	passively aerated composting	
	Sayan Tanpanich, Rewat Jindajia and Soonthorn Duriyaprapan	
P-04	Flood-risk mapping of watershed areas in Northeast Thailand using	80
	Multi-temporal RADARSAT Data	
	Tussaporn Thanajaturon and Charat Mongkolsawat	
P-05	Ecosystem diversity in The Phu Luang Wildlife Sanctuary, Northeast	81
5 (55)	Thailand: Satellite data and GIS applications	
	Urawan Chanket and Charat Mongkolsawat	
P-06	Calculation of electronic structures and magnetic properties	82
	of MgO with and without transition metal elements (Mn,Fe,Co)	02
	Ekaphan Swatsitang, Sutisa Banyong and Sriprajak Krongsuk	
P-07	Effect of Ti doping on the electrical and giant dielectric properties	83
,	of (Li,Ti)-doped NiO ceramics prepared by a simple PVA sol-gel method	
	Prasit Thongbai, Teerapon Yamwong and Santi Maensiri	
P-08	Solar photocatalytic oxidation of trichlorophenols using	84
1 00	titanium dioxide	04
	Somkiat Srijaranai and Naramon Homewong	
P-09	Sorption of acid yellow 42 on silk fibers from aqueous solutions	85
1 07	Suta Poosittisak, Tavatchai Sripakdee, Kitti Akampon and	0.0
	Kitti Amornraksa	
P-10	Screening of chemicals composition in <i>Eucalyptus</i> wood vinegar as	86
r-10	antioxidant agents	80
	Chalerm Ruangviriyachai, Morakot Tupjun, Manop Sriuttha,	
	Panadda Tansupo and Saksit Chanthai	
P-11	Excessive exposure of monosodium glutamate affects stress	07
r-11		87
	responded protein pattern in neonatal adrenal gland	
D 12	Anuwat Wanthong, Sompong Tammasirirak and Khomsorn Lomthaisong	0.0
P-13	Chemical constituents from Fungus Eurotium Chevalieri	88
P. 14	Ruchiruttikorn Suwannatrai, Kwanjai Kanokmedhakul,	
	Somdej Kanokmedhakul, Kasem Soytong, Samran Prabpai	
	and Palangpol Kongsaeree	250
P-14	Lignolytic enzymes of bacterial strains	89
	Wiyada Mongkolthanaruk	223
P-15	Enumeration of microbes in liquid fertilizer	90
	Nuntavun Riddech	



AMEC-6

The 6th Asian Meeting on Electroceramics

The 28th Electronics Division Meeting of CSJ (CSJ) 第28回 エレクトロセラミックス研究討論会)

October 22-24, 2008 Tsukuba, Japan

Organized by

Electronics Division of the Ceramic Society of Japan National Institute for Materials Science (NIMS)





Giant Dielectric Permittivity observed in Li and Fe doped NiO

(Department of Physic, Faculty of Science, Khon Kaen University, Khon Kaen, 40002, Thailand)
P. Thongbai*, S. Maensiri,

(National Metals and Materials Technology Center (MTEC), Thailand Science Park, Pathumthani, 12120,
Thailand) T. Yamwong

E-mail: prasitphysics@hotmail.com

This work first reports the high dielectric response in $\text{Li}_x\text{Fe}_y\text{Ni}_{1-x-y}\text{O}$ (LFNO) ceramics, i.e., $\varepsilon' \sim 10^3$ - 10^4 . The phase formation and microstructure of the sintered samples were studied by XRD and SEM, respectively. The dielectric properties as a function of frequencies (10^2 - 10^6 Hz) were investigated over temperature a range of -50 to 100°C . Our results indicated that the concentrations of Li and Fe have remarkable effects on the dielectric properties of the LFNO ceramics. The dielectric permittivity increased with increasing Li concentration and it decreased when the concentration of Fe increased. The analysis of complex impedance spectroscopy suggested that these LFNO ceramics were electrically heterogeneous consisting of semeconducting grain and insulating grain boundary. It can be proposed that such a high apparent dielectric permittivity observed in these LFNO ceramics is attributed to the Maxwell-Wagner polarization mechanism and thermally activated mechanism.

RESULTS

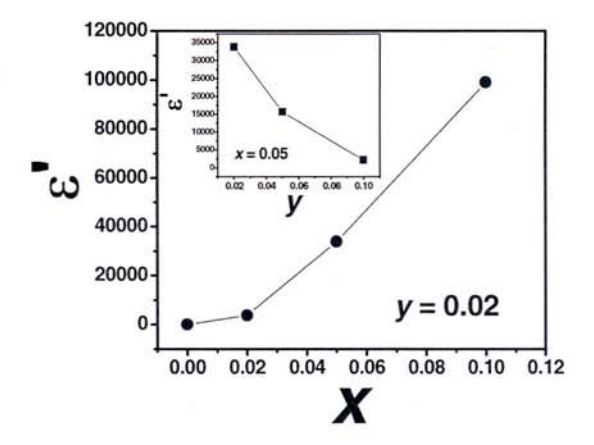


Fig. 1 The dependence of the dielectric constant at room temperature and 1 kHz on the concentration of Li and Ti (see in the inset) doped in $\text{Li}_x\text{Fe}_v\text{Ni}_{1-x-y}\text{O}$ ceramics.

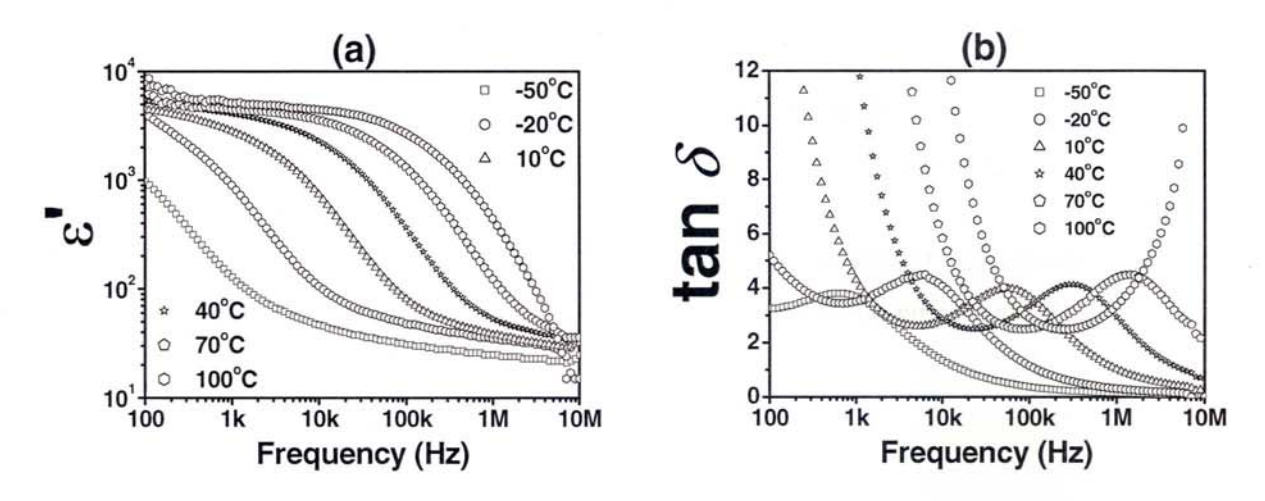


Fig. 2 The frequency dependence of (a) dielectric constant ε' and (b) loss tangent $\tan \delta$ at various temperatures for $\text{Li}_{0.02}\text{Fe}_{0.02}\text{Ni}_{0.96}\text{O}$ ceramic.

AMEC-6(Oct.22-24.2008) 279

14:50 O-3B-07

Scaling Behavior of Sub-Coercive Field Dynamic Hysteresis in BaTiO₃ Single Crystal *N. Wongdamnern, A. Ngamjarurojana, S. Ananta, Y. Laosiritaworn, R. Yimnirun (*Chiang Mai University, Thailand)

15:10 O-3B-08

Enhancement of Dielectric properties of Low Temperature Sintering Ba_{0.6}Sr_{0.4}TiO₃ Thick Film by Isostatic Pressing Technique

*Minghui Zhang, Hong Wang, Huanfu Zhou, Feng Xiang, Xi Yao

(*Xi'an Jiaotong University, China)

15:30 Break

Room: B Dielectric, ferroelectric & Piezoelectric ceramics (4)

(Chair-persons: H. Maiwa, Shonan Inst. of Tedch., and T. Bongkarn, Naresuan Univ.)

15:50 O-3B-09

Structural, Dielectric and Ferroelectric Properties of Ternary BaTiO₃-CaTiO₃-SrTiO₃ Ceramics *Xusheng Wang, Lingling Zhang, Xi Yao (*Tongji University, China)

16:10 O-3B-10

Giant Dielectric Permittivity observed in Li and Fe doped NiO *P. Thongbai, S. Maensiri, T. Yamwong (*Khon Kaen University, Thailand)

16:30 O-3B-11

Aging effect in paraelectric state of ferroelectrics
*Dezhen Xue, Xiaobing Ren (*National Institute for Materials Science, Japan)

16:50 O-3B-12

Dynamics of Central Peaks in the Brillouin Scattering Spectra of Relaxor Ferroelectrics *G. Shabbir, S. Kojimal, J. Bashir (*Pakistan Institute of Nuclear Science & Technology, Pakistan)

Room: C MLCC Technology (3)

(Chair-persons: S. Sato, TDK Corp.)

14:00 I-3C-02 (Invited)

0-3C-06

High Temperature Guaranteed Multilayer Ceramic Capacitors for automotive applications

*Hiroshi Takagi (*Murata Mfg. Co.,Ltd., Japan)

Size Effect and Domain Contribution of Barium Titanate Ceramics

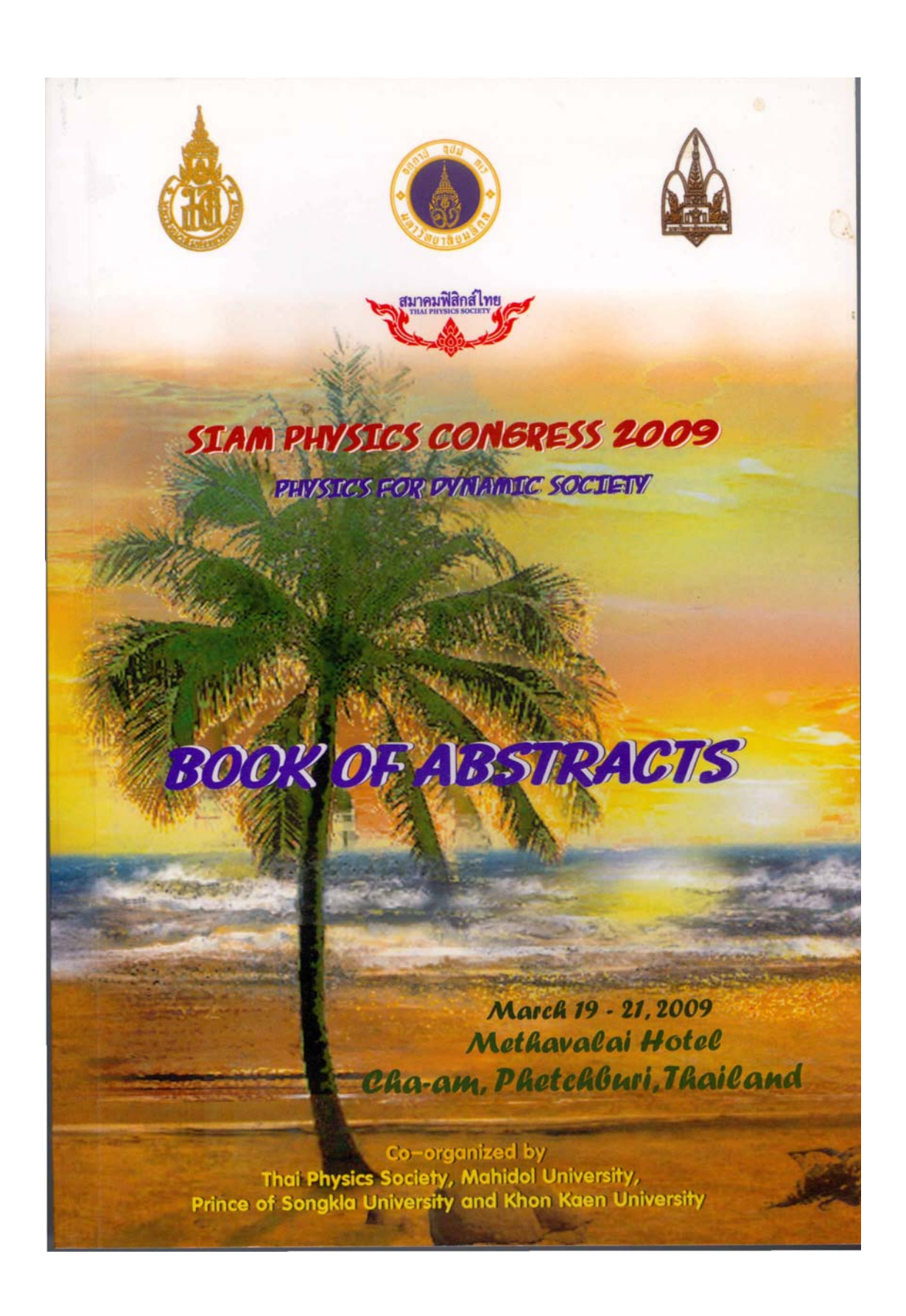
*Takaaki Tsurumi, Takuya Hoshina (*Tokyo Institute of Technology, Japan)

14:50 O-3C-07

14:30

Atomic and Electronic Structures of BaTiO₃ Ceramic Nanoclusters: Theoretical Study *Shin'ichi Higai, Atsushi Honda, Keisuke Kageyama, Hiroshi Takagi, Yukio Sakabe, Hiroki

Moriwake (*Murata Mfg. Co., Ltd., Japan)



MP_O4	Experiments of Longitudinal Magnetic Filtration Were Performed With Wastewater Sample of Fe powder Dispersing in Water Pipes Flowing With A Constant Velocity Kampan Wiangnon, Ubon Ratchathani University	67
MP_O5	The wettability of PET treated by O ₂ , N ₂ and Ar plasmas by capillary rise method. Kanchit Kamlangkla, Chulalongkorn University	68
MP_O6	Synthesis and Characterization of SnO ₂ Nanostructures by Thermal-Carbon Assisted Kiattisak Noipa, <i>Ubon Ratchathani University</i>	69
MP_O7	Growth and characterization of pure and K* doped Zinc Thiourea Chloride single crystals Nakarin Pattanaboonmee, Suranaree University of Technology	70
MP_O8	Effect growth pressure on diameter of carbon nanotubes prepared from n-hexane Naratip Songmee, Chiang Mai University	71
MP_O9	Physical Properties of Ruddlesden-Popper of $Sr_3Fe_{2-x}Mn_xO_{7-\delta}$ (x = 0.2, 0.4, 0.6, 0.8, 1.0) Palin Sittipon, Suranaree University of Technology	72
MP_O10	Effect of Organoclay Surface Coverage on the Formation of Polypropylene-Clay Nanocomposite Fibers Prepared by Melt- Spin Pantisa Ruenpakdan, Mahidol University	73
MP_O11	Effects of Insulating Layers and Dc bias on Dielectric Relaxation Behavior of Li _{0.05} Fe _{0.10} Ni _{0.85} O Polycrystalline Ceramic Prasit Thongbai, Khon Kaen University	74
MP_O12	Synthesis and Characterization of CuO nanowires by Thermal Evaporation Method Pristanuch Kasian, Ubon Ratchathani University	75
MP_O13	Palaeointensity Determination on Ancient Bricks from Southern Thailand Suriyan Promduang, Prince of Songkla University	76
MP_O14	Synthesis and characterization of non-cytotoxic magnetic nanoparticles La _{0.75} Sr _{0.25} MnO ₃ by simple thermal hydro-decomposition Sujittra Daengsakul, Khon Kaen University	77
MP_O15	Mineralogy, Chemical Analyses and Ceramic Properties of Clays in Southern Thailand Used in Ceramics Industry Sunaree Bordeepong, Prince of Sonokla University	78

Effects of Insulating Layers and Dc bias on Dielectric Relaxation Behavior of Li_{0.05}Fe_{0.10}Ni_{0.85}O Polycrystalline Ceramic

P. Thongbail*, T. Yamwong2, and S. Maensiri1

¹Integrated Nanotechnology Research Center (INRC), and Small & Strong Materials Group (SSMG), Department of Physics, Khon Kaen University, Khon Kaen, 40002, Thailand

²National Metals and Materials Technology Center (MTEC), Thailand Science Park, Pathumthani, 12120, Thailand

Abstract

We reported the effects of insulating layers and dc bias on the dielectric relaxation behavior of high-permittivity Li_{0.05}Fe_{0.10}Ni_{0.85}O (LFNO) polycrystalline ceramic prepared by a polymer pyrolysis route. The dielectric properties of the asand polished-LFNO samples were studied as functions of temperature (-50-200 °C), frequency (10²-10⁷ Hz), and dc bias (0-20 V). The phase composition and microstructure were characterized by X-ray diffraction (XRD) and scanning electron microscopy (SEM) with energy dispersive X-ray spectrometer (EDS), respectively. Analysis of microstructure and phase composition revealed that the LFNO ceramic exhibited a core/shell structure and the second phase of NiFe₂O₄ existed as the grain boundary. It was found that the insulating surface-layer had an influence on the high dielectric properties of the LFNO sample, but the relaxation behavior. Our results indicated that the applied voltage had significant effects on the electrical responses of the insulating surface-layer and grain boundary layers. The resistances of the surface-layer and grain boundary decreased with an increase in the applied voltage, whereas the bulk resistance remained constant. The high dielectric properties of the LFNO sample were ascribed based on the space charge polarization at the insulating layers. The close relationship between the dielectric relaxation mechanism and the electrical transport inside the grains was observed.

Keyword: Dielectric properties, Dielectric loss and relaxation, Scanning electron microscopy

Corresponding author. Email: prasitphysics@hotmail.com